Progress in Particle and Nuclear Physics 66 (2011) 519–548

Contents lists available at ScienceDirect

Progress in Particle and Nuclear Physics

journal homepage: www.elsevier.com/locate/ppnp

Review

Relativistic nuclear energy density functionals: Mean-field and beyond

T. Nikšić [a], D. Vretenar [a,*], P. Ring [b]

[a] Physics Department, Faculty of Science, University of Zagreb, 10000 Zagreb, Croatia

[b] Physik-Department der Technischen Universität München, D-85748 Garching, Germany

ARTICLE INFO

Keywords:
Nuclear structure
Nuclear density functional theory and extensions
Collective correlations

ABSTRACT

Relativistic energy density functionals (EDF) have become a standard tool for nuclear structure calculations, providing a complete and accurate, global description of nuclear ground states and collective excitations. Guided by the medium dependence of the microscopic nucleon self-energies in nuclear matter, semi-empirical functionals have been adjusted to the nuclear matter equation of state and to bulk properties of finite nuclei, and applied to studies of arbitrarily heavy nuclei, exotic nuclei far from stability, and even systems at the nucleon drip-lines. REDF-based structure models have also been developed that go beyond the static mean-field approximation, and include collective correlations related to the restoration of broken symmetries and to fluctuations of collective variables. These models are employed in analyses of structure phenomena related to shell evolution, including detailed predictions of excitation spectra and electromagnetic transition rates.

Contents

* Corresponding author.
E-mail address: vretenar@phy.hr (D. Vretenar).

0146-6410/$ – see front matter © 2011 Elsevier B.V. All rights reserved.
doi:10.1016/j.ppnp.2011.01.055

1. Introduction

Nuclear energy density functionals (EDF) presently provide the most complete and accurate description of ground-state properties and collective excitations over the whole nuclide chart. Among the microscopic approaches to the nuclear many-body problem, probably no other method achieves comparable global accuracy at the same computational cost, and it is the only one that can describe the evolution of structure phenomena from relatively light systems to superheavy nuclei, and from the valley of β-stability to the particle drip-lines [1,2].

In practical implementations the EDF framework is realized on two specific levels. The basic implementation is in terms of self-consistent mean-field (SCMF) models, in which an EDF is constructed as a functional of one-body nucleon density matrices that correspond to a single product state—the Slater determinant of single-particle or single-quasiparticle states. The SCMF approach to nuclear structure is analogous to the Kohn–Sham density functional theory (DFT) [3,4]. DFT enables a description of quantum many-body systems in terms of a universal energy density functional. Universal in the sense that, for a given inter-particle interaction, it has the same functional form for all systems. Nuclear SCMF models effectively map the many-body problem onto a one-body problem, and the exact EDF is approximated by simple, mostly analytical, functionals of powers and gradients of ground-state nucleon densities and currents, representing distributions of matter, spins, momentum and kinetic energy. In principle the nuclear EDF can incorporate short-range correlations related to the repulsive core of the inter-nucleon interaction, and long-range correlations mediated by nuclear resonance modes. Even though it originates in the effective interaction between nucleons, a generic density functional is not necessarily related to any given nucleon–nucleon (NN) potential and, in fact, some of the most successful modern functionals are entirely empirical. Of course it would be desirable to have a fully microscopic foundation for a universal density functional, and this is certainly one of the major challenges for the framework of nuclear EDFs. Because it includes correlations, the self-consistent Kohn–Sham approach goes beyond the Hartree–Fock approximation, and it also has the advantage of being a local scheme. Its usefulness, however, crucially depends on our ability to construct accurate approximations for the most important part of the functional, that is, the universal exchange–correlation functional [5]. In an "ab initio" approach one might start from a Hamiltonian that describes two-nucleon and few-body scattering and bound-state observables [6], or an effective field theory of low-energy in-medium NN interactions can be used to build approximations to the exact exchange–correlation functional [7]. However, even if a fully microscopic EDF is eventually developed, the parameters of that functional will still have to be fine tuned to structure data of finite nuclei. This is because data on nucleon–nucleon scattering and few-nucleon systems, or gross properties of infinite nuclear matter, cannot determine the density functional to a level of accuracy necessary for a quantitative description of medium-heavy and heavy nuclei.

When considering applications, however, an important challenge for the framework of EDF is the systematic treatment of collective correlations related to restoration of broken symmetries and fluctuations in collective coordinates. A static nuclear EDF is of course characterized by symmetry breaking—translational, rotational, particle number, and can only provide an approximate description of bulk ground-state properties. To calculate excitation spectra and electromagnetic transition rates in individual nuclei, it is necessary to extend the Kohn–Sham EDF framework, that is the SCMF scheme, to include correlations that arise from symmetry restoration and fluctuations around the mean-field minimum. Collective correlations are sensitive to shell effects, display pronounced variations with particle number and, therefore, cannot be incorporated in a universal EDF. On the second level that takes into account collective correlations through the restoration of broken symmetries and configuration mixing of symmetry-breaking product states, the many-body energy takes the form of a functional of all transition density matrices that can be constructed from the chosen set of product states. This set is chosen to restore symmetries or/and to perform a mixing of configurations that correspond to specific collective modes using, for instance, the (quasiparticle) random-phase approximation (QRPA) or the Generator Coordinate Method (GCM). The latter includes correlations related to finite-size fluctuations in a collective degree of freedom, and can be also used to restore selection rules that are crucial for spectroscopic observables.

An important class of nuclear structure models belongs to the framework of relativistic energy density functionals. In particular, a number of very successful relativistic mean-field (RMF) models have been constructed based on the framework of quantum hadrodynamics (QHD) [8,9]. There are important advantages in using functionals with manifest covariance [10]. The most obvious is the natural inclusion of the nucleon spin degree of freedom, and the resulting nuclear spin–orbit potential which emerges automatically with the empirical strength in a covariant formulation. The consistent treatment of large, isoscalar, Lorentz scalar and vector self-energies provides a unique parametrization of time–odd components of the nuclear mean-field, i.e. nucleon currents, which is absent in the non-relativistic representation of the energy density functional. The empirical pseudospin symmetry in nuclear spectroscopy finds a natural explanation in terms of relativistic mean fields [11]. On a microscopic level, it has been argued [10] that a covariant formulation of nuclear dynamics manifests the true energy scales of QCD in nuclei, and is consistent with the nonlinear realization of chiral symmetry through the implicit inclusion of pion-nucleon dynamics in the effective nucleon self-energies. A covariant treatment of nuclear matter provides a distinction between scalar and four-vector nucleon self energies, leading to a very natural saturation mechanism.

RMF-based models have been very successfully employed in analyses of a variety of nuclear structure phenomena, not only in nuclei along the valley of β-stability, but also in exotic nuclei with extreme isospin values and close to the particle drip lines. Applications have reached a level of sophistication and accuracy comparable to the non-relativistic Hartree–Fock–Bogoliubov approach based on Skyrme functionals or Gogny effective interactions [2,12–14]. Relativistic EDFs have mostly been applied in the description of ground-state properties and excitation energies of giant resonance

at the self-consistent mean-field level, taking into account pairing correlations in open-shell nuclei in the Hartree–(Fock)–Bogoliubov framework, and performing consistent (Q)RPA calculations of small-amplitude collective motion. However, for relativistic structure models to make detailed spectroscopic predictions, symmetries broken by the static nuclear mean field must be restored, and fluctuations around the mean-field minimum must be taken into account. While symmetry restoration and configuration mixing calculations have routinely been applied with non-relativistic density functionals for many years, it is only more recently that these type of structure models have been developed using relativistic density functionals [15–19].

In this work we review recent advances in the framework of relativistic EDFs and, in particular, the latest extensions that include the treatment of collective correlations. Section 2 introduces the general framework of REDFs. In Section 3 we review a class of semi-empirical functionals and, in particular, the functional DD-PC1 that will be used in illustrative calculations throughout this work. For a quantitative analysis of open-shell nuclei it is necessary to consider pairing correlations, and in Section 4 we introduce the relativistic Hartree–Bogoliubov model for triaxial nuclei, with a separable pairing interaction. The treatment of collective correlations is reviewed and illustrated with a number of examples in Section 5 (symmetry restoration and configuration mixing calculations) and in Section 6 (collective Hamiltonian in five dimensions). Section 7 summarizes the results and ends with an outlook for future studies.

2. Relativistic energy density functionals

2.1. Quantum hadrodynamics

In conventional quantum hadrodynamics (QHD) [8,9] a nucleus is described as a system of Dirac nucleons coupled to exchange mesons through an effective Lagrangian. The isoscalar scalar σ meson, the isoscalar vector ω meson, and the isovector vector ρ meson build the minimal set of meson fields that, together with the electromagnetic field, is necessary for a description of bulk and single-particle nuclear properties. In the *mean-field* approximation the meson-field operators are replaced by their expectation values in the nuclear ground state. In addition, a quantitative treatment of nuclear matter and finite nuclei necessitates a medium dependence of effective mean-field interactions that takes into account higher-order many-body effects. A medium dependence can either be introduced by including nonlinear meson self-interaction terms in the Lagrangian, or by assuming an explicit density dependence for the meson–nucleon couplings. The former approach has been adopted in the construction of several successful phenomenological RMF interactions, for instance, the very popular NL3 [20], or the more recent PK1, PK1R [21] and FSUGold [22] parameterizations of the effective Lagrangian. In the latter case, the density dependence of the meson–nucleon vertex functions can be parameterized starting from microscopic Dirac–Brueckner calculations of symmetric and asymmetric nuclear matter [23–25] or it can be fully phenomenological [26–28], with parameters adjusted to data on finite nuclei and empirical properties of symmetric and asymmetric nuclear matter.

At the energy scale characteristic for nuclear binding and low-lying excited states, meson exchange (σ, ω, ρ, ...) is just a convenient representation of the effective nuclear interaction. The exchange of heavy mesons is associated with short-distance dynamics that cannot be resolved at low energies, and therefore in each channel (scalar-isoscalar, vector-isoscalar, scalar-isovector, and vector-isovector) meson exchange can be replaced by the corresponding local four-point (contact) interactions between nucleons. The self-consistent relativistic mean-field framework can be formulated in terms of point-coupling nucleon interactions. When applied in the description of finite nuclei, relativistic mean-field point-coupling (RMF-PC) models [29–33] produce results that are equivalent to those obtained in the meson exchange picture. Of course, also in the case of contact interactions, medium effects can be taken into account by the inclusion of higher-order interaction terms, for instance, six-nucleon vertices $(\bar{\psi}\psi)^3$, and eight-nucleon vertices $(\bar{\psi}\psi)^4$ and $[(\bar{\psi}\gamma_\mu\psi)(\bar{\psi}\gamma^\mu\psi)]^2$, or it can be encoded in the effective couplings, i.e. in the density dependence of strength parameters of the interaction in the isoscalar and isovector channels. Although a number of point-coupling models have been developed over the years, it is only more recently that phenomenological parameterizations have been adjusted and applied in the description of finite nuclei on a level of accuracy comparable to that of standard meson-exchange effective interactions [33,34].

The relation between the two representations: finite-range (meson exchange) and zero-range (point-coupling), is straightforward in nuclear matter because of constant nucleon scalar and vector densities. The Klein–Gordon equations of the meson-exchange model with meson masses m_ϕ and density-dependent couplings $g_\phi(\rho)$, are replaced by the corresponding point-coupling interaction terms with strength parameters g_ϕ^2/m_ϕ^2. In finite nuclei, however, the problem is not so simple. Because of the radial dependence of the densities, the expansion of the meson propagator in terms of $1/m_\phi^2$ leads to an infinite series of gradient terms. In practice this series has to be replaced by a finite number of terms with additional phenomenological parameters adjusted to low-energy data. A number of studies have shown that, both for finite-range and for point-coupling mean-field models, the empirical data set of ground-state properties of finite nuclei can determine only a relatively small number of parameters in the general expansion of the effective Lagrangian in powers of the fields and their derivatives. It is therefore not a priori clear how to select the set of point-coupling interaction terms that will describe structure properties at the same level of accuracy as the meson-exchange models. The mapping of a phenomenological finite-range interaction with density-dependent meson–nucleon couplings (DD-ME2) on the zero-range (point-coupling) relativistic mean-field framework was considered in Ref. [35]. A family of point-coupling

effective interactions was constructed with different values of the strength parameter of the isoscalar–scalar derivative term. In the meson-exchange picture this corresponds to different values of the σ-meson mass. The parameters of the isoscalar–scalar and isovector–vector channels of the point-coupling interactions were adjusted to nuclear matter and ground-state properties of finite nuclei. By comparing results for infinite and semi-infinite nuclear matter, ground-state masses, charge radii, and collective excitations, constraints were placed on the parameters of phenomenological point-coupling relativistic effective interaction.

2.2. Elements of density functional theory

Density Functional Theory (DFT) is one of the most popular and successful "ab initio" approaches to the structure of quantum many-body systems (atoms, molecules, solids). Probably no other method achieves comparable accuracy at the same computational cost. The basic concept is that the ground-state properties of a stationary many-body system can be represented in terms of the ground-state density alone. Since the density $\rho(\mathbf{r})$ is a function of only three spatial coordinates, rather than the $3N$ coordinates of the N-body wave function, DFT is computationally feasible even for large systems.

Most practical applications of Density Functional Theory use the effective single-particle Kohn–Sham (KS) equations [3,4], introduced for an auxiliary system of N non-interacting particles. According to the Hohenberg–Kohn theorem [36], there exists a unique energy functional

$$E_s[\rho] = T_s[\rho] + \int \mathrm{d}^3 r\, v_s(\mathbf{r})\rho(\mathbf{r}), \tag{1}$$

for which the variational equation yields the exact ground-state density $\rho_s(\mathbf{r})$. $T_s[\rho]$ is the universal kinetic energy functional of the non-interacting system. The KS scheme is based on the following assertion: for any interacting system, there exists a unique local single-particle potential $v_s(\mathbf{r})$, such that the exact ground-state density of the interacting system equals the ground-state density of the auxiliary non-interacting system:

$$\rho(\mathbf{r}) = \rho_s(\mathbf{r}) = \sum_i^N |\phi_i(\mathbf{r})|^2, \tag{2}$$

expressed in terms of the N lowest occupied single-particle orbitals—solutions of the Kohn–Sham equations:

$$\left[-\nabla^2/2m + v_s(\mathbf{r})\right]\phi_i(\mathbf{r}) = \varepsilon_i\phi_i(\mathbf{r}). \tag{3}$$

The uniqueness of $v_s(\mathbf{r})$ follows from the Hohenberg–Kohn theorem and the single-particle orbitals are unique functionals of the density: $\phi_i(\mathbf{r}) = \phi_i([\rho]; \mathbf{r})$.

For a self-bound system like the atomic nucleus, the energy functional can be decomposed into three separate terms:

$$F[\rho] = T_s[\rho] + E_H[\rho] + E_{xc}[\rho], \tag{4}$$

where T_s is the kinetic energy of the non-interacting A-nucleon system, E_H is a Hartree energy, and E_{xc} denotes the exchange–correlation energy which, by definition, contains everything else—all the many-body effects. The corresponding local exchange–correlation potential is defined by:

$$v_{xc}[\rho](\mathbf{r}) = \frac{\delta E_{xc}[\rho]}{\delta\rho(\mathbf{r})}, \tag{5}$$

and thus

$$v_s[\rho](\mathbf{r}) = v_H[\rho](\mathbf{r}) + v_{xc}[\rho](\mathbf{r}). \tag{6}$$

Since the effective potential depends on the ground-state density, the system of Eqs. (2), (3) and (6) has to be solved self-consistently. This is the Kohn–Sham scheme of density functional theory [3]. By including correlation effects the KS framework goes beyond the Hartree–Fock approximation but, in addition, it has the advantage of being a *local* scheme. It is clear, however, that the usefulness of the Kohn–Sham scheme crucially depends on our ability to construct accurate approximations to the exact exchange–correlation energy. The true exchange–correlation energy functional is *universal*, i.e. given the inter-particle interaction, it has the same functional form for all systems. One possible approach is to develop E_{xc} from first principles by incorporating known exact constraints. Another is empirical, a parametric ansatz is optimized by adjusting it to a set of data.

The Hohenberg–Kohn theorem and the self-consistent Kohn–Sham scheme are straightforwardly extended to the relativistic domain [5]. The relativistic Kohn–Sham equation for the auxiliary non-interacting system is represented by the single-particle Dirac equation with a local four-potential that depends on the ground-state four-current.

2.3. Empirical nuclear density functionals

At the energy and momentum scales characteristic of nuclei, the only degrees of freedom that have to be taken into account explicitly in the description of many-body dynamics are pions and nucleons. The behavior of the nucleon–nucleon (NN) interaction at long and intermediate distances is determined by one- and two-pion exchange processes. As already

emphasized, short-distance dynamics cannot be resolved at low energies that characterize nuclear binding and, therefore, it is represented by local four-point (contact) NN interactions, with low-energy (medium-dependent) parameters adjusted to nuclear data. These concepts of effective field theory and density functional theory methods have recently been used to derive a microscopic relativistic energy density functional framework constrained by in-medium QCD sum rules and chiral symmetry [37,38]. The density dependence of the effective nucleon–nucleon couplings is determined from the long- and intermediate-range interactions generated by one- and two-pion exchange processes. They are computed using in-medium chiral perturbation theory, explicitly including $\Delta(1232)$ degrees of freedom [39]. Regularization dependent contributions to the energy density of nuclear matter, calculated at the three-loop level, are absorbed in contact interactions with parameters representing unresolved short-distance dynamics.

In this work we review a class of relativistic energy density functionals (REDFs) similar to that introduced in Refs. [37,38] but, instead of using low-energy QCD constraints for the medium dependence of the parameters, a phenomenological ansatz is adjusted exclusively to data on nuclear ground states. This empirical approach, although guided by microscopic nucleon self-energies in nuclear matter, gives us more freedom to investigate in detail the relationship between global properties of a nuclear matter equation of state (volume, surface, and asymmetry energies) and the corresponding predictions for properties of finite nuclei.

The basic building blocks of a relativistic nuclear energy density functional are the densities and currents bilinear in the Dirac spinor field ψ of the nucleon:

$$\bar{\psi}\mathcal{O}_\tau\Gamma\psi, \quad \mathcal{O}_\tau \in \{1, \tau_i\}, \ \Gamma \in \{1, \gamma_\mu, \gamma_5, \gamma_5\gamma_\mu, \sigma_{\mu\nu}\}. \tag{7}$$

Here τ_i are the isospin Pauli matrices and Γ generically denotes the Dirac matrices. The nuclear ground-state density and energy are determined by the self-consistent solution of relativistic linear single-nucleon Kohn–Sham equations. To derive those equations it is useful to construct an interaction Lagrangian with four-fermion (contact) interaction terms in the various isospace–space channels:

$$\begin{aligned}
&\text{isoscalar–scalar}: \ (\bar{\psi}\psi)^2\\
&\text{isoscalar–vector}: \ (\bar{\psi}\gamma_\mu\psi)(\bar{\psi}\gamma^\mu\psi)\\
&\text{isovector–scalar}: \ (\bar{\psi}\vec{\tau}\psi)\cdot(\bar{\psi}\vec{\tau}\psi)\\
&\text{isovector–vector}: \ (\bar{\psi}\vec{\tau}\gamma_\mu\psi)\cdot(\bar{\psi}\vec{\tau}\gamma^\mu\psi).
\end{aligned}$$

Vectors in isospin space are denoted by arrows. A general Lagrangian can be written as a power series in the currents $\bar{\psi}\mathcal{O}_\tau\Gamma\psi$ and their derivatives, with higher-order terms representing in-medium many-body correlations [29–33]. The problem however, as already emphasized, is that the empirical data set of bulk and single-particle properties of finite nuclei can only constrain a relatively small set of parameters in the general expansion of an effective Lagrangian. An alternative, that directly leads to linear single-nucleon Kohn–Sham equations, is to construct a Lagrangian with second-order interaction terms only, with many-body correlations encoded in density-dependent coupling functions [37,38]. In complete analogy to the successful meson-exchange RMF phenomenology, in which the isoscalar–scalar σ meson, the isoscalar–vector ω meson, and the isovector–vector ρ meson build the minimal set of meson fields that is necessary for a quantitative description of nuclei, an effective Lagrangian that includes the isoscalar–scalar, isoscalar–vector and isovector–vector four-fermion interactions reads:

$$\begin{aligned}
\mathcal{L} = {} & \bar{\psi}(\mathrm{i}\gamma\cdot\partial - m)\psi - \frac{1}{2}\alpha_S(\hat{\rho})(\bar{\psi}\psi)(\bar{\psi}\psi) - \frac{1}{2}\alpha_V(\hat{\rho})(\bar{\psi}\gamma^\mu\psi)(\bar{\psi}\gamma_\mu\psi)\\
& - \frac{1}{2}\alpha_{\mathrm{TV}}(\hat{\rho})(\bar{\psi}\vec{\tau}\gamma^\mu\psi)(\bar{\psi}\vec{\tau}\gamma_\mu\psi) - \frac{1}{2}\delta_S(\partial_\nu\bar{\psi}\psi)(\partial^\nu\bar{\psi}\psi) - e\bar{\psi}\gamma\cdot A\frac{(1-\tau_3)}{2}\psi.
\end{aligned} \tag{8}$$

In addition to the free-nucleon Lagrangian and the point-coupling interaction terms, when applied to nuclei, the model must include the coupling of the protons to the electromagnetic field. The derivative term in Eq. (8) accounts for leading effects of finite-range interactions that are crucial for a quantitative description of nuclear density distribution, e.g. nuclear radii. Similar interactions can be included in each space–isospace channel, but in practice data only constrain a single derivative term, for instance $\delta_S(\partial_\nu\bar{\psi}\psi)(\partial^\nu\bar{\psi}\psi)$. The inclusion of an adjustable derivative term only in the isoscalar–scalar channel is consistent with conventional meson-exchange RMF models, in which the mass of the fictitious σ meson is adjusted to nuclear matter and ground-state properties of finite nuclei, whereas free values are used for the masses of the ω and ρ mesons.

The point-coupling Lagrangian equation (8) does not include isovector–scalar terms. In the meson-exchange picture this channel is represented by the exchange of an effective δ meson, and its inclusion introduces a proton–neutron effective mass splitting and enhances the isovector spin–orbit potential. Although the spin–orbit strength has a relatively well-defined value, the distribution between the scalar and vector channels is not determined by ground-state data. To reduce the number of adjustable parameters, the isovector–scalar channel may be omitted from an energy density functional that will primarily be used for the description of low-energy nuclear structure.

In general the strength parameters of the interaction terms in Eq. (8) are functions of the nucleon 4-current:

$$j^\mu = \bar{\psi}\gamma^\mu\psi = \hat{\rho}u^\mu, \tag{9}$$

where u^μ is the 4-velocity defined as $(1-\boldsymbol{v}^2)^{-1/2}(1,\boldsymbol{v})$. In the rest-frame of homogeneous nuclear matter: $\boldsymbol{v}=0$. The single-nucleon Dirac equation, the relativistic analogue of the Kohn–Sham equation, is obtained from the variation of the Lagrangian with respect to $\bar{\psi}$:

$$\left[\gamma_\mu(\mathrm{i}\partial^\mu - \Sigma^\mu - \Sigma_R^\mu) - (m+\Sigma_S)\right]\psi = 0, \tag{10}$$

with the nucleon self-energies defined by the following relations:

$$\Sigma^\mu = \alpha_V(\rho_v)j^\mu + e\frac{(1-\tau_3)}{2}A^\mu \tag{11}$$

$$\Sigma_R^\mu = \frac{1}{2}\frac{j^\mu}{\rho_v}\left\{\frac{\partial\alpha_S}{\partial\rho}\rho_s^2 + \frac{\partial\alpha_V}{\partial\rho}j_\mu j^\mu + \frac{\partial\alpha_{\mathrm{TV}}}{\partial\rho}\vec{j}_\mu\vec{j}^\mu\right\} \tag{12}$$

$$\Sigma_S = \alpha_S(\rho_v)\rho_s - \delta_S\Box\rho_s \tag{13}$$

$$\Sigma_{\mathrm{TV}}^\mu = \alpha_{\mathrm{TV}}(\rho_v)\vec{j}^\mu. \tag{14}$$

In addition to the contributions of the isoscalar–vector four-fermion interaction and the electromagnetic interaction, the isoscalar–vector self-energy Σ^μ includes the "rearrangement" terms Σ_R^μ, arising from the variation of the vertex functionals α_S, α_V, and α_{TV} with respect to the nucleon fields in the density operator $\hat{\rho}$. The inclusion of the rearrangement self-energy is essential for energy–momentum conservation and the thermodynamical consistency of the model [23,26,27]. Σ_S and Σ_{TV}^μ denote the isoscalar–scalar and isovector–vector self-energies, respectively.

In the relativistic density functional framework the nuclear ground state $|\phi_0\rangle$ is represented by the self-consistent mean-field solution of the system of Eqs. (10)–(14), with the isoscalar and isovector 4-currents and scalar density:

$$j_\mu = \langle\phi_0|\bar{\psi}\gamma_\mu\psi|\phi_0\rangle = \sum_{k=1}^{N} v_k^2\bar{\psi}_k\gamma_\mu\psi_k, \tag{15}$$

$$\vec{j}_\mu = \langle\phi_0|\bar{\psi}\gamma_\mu\vec{\tau}\psi|\phi_0\rangle = \sum_{k=1}^{N} v_k^2\bar{\psi}_k\gamma_\mu\vec{\tau}\psi_k, \tag{16}$$

$$\rho_S = \langle\phi_0|\bar{\psi}\psi|\phi_0\rangle = \sum_{k=1}^{N} v_k^2\bar{\psi}_k\psi_k, \tag{17}$$

where ψ_k are Dirac spinors, and the sum runs over occupied positive-energy single-nucleon orbitals, including the corresponding occupation factors v_k^2. The single-nucleon Dirac equations are solved self-consistently in the "no-sea" approximation that omits the explicit contribution of negative-energy solutions of the relativistic equations to the densities and currents. Vacuum polarization effects are implicitly included in the adjustable density-dependent parameters of the theory.

To determine the density dependence of the coupling functionals α_S, α_V, and α_{TV} one could start from a microscopic (relativistic) equation of state (EoS) of symmetric and asymmetric nuclear matter, and map the corresponding nucleon self-energies on the mean-field self-energies Eqs. (11)–(14) that determine the single-nucleon Dirac equation (10). This approach has been adopted, for instance, in RMF models based on Dirac–Brueckner–Hartree–Fock self-energies in nuclear matter [23–25], or on in-medium chiral perturbation theory (ChPT) calculations of the nuclear matter EoS [37,38]. In general, however, energy density functionals determined directly from a microscopic EoS do not provide a very accurate description of data in finite nuclei. The reason, of course, is that a calculation of the nuclear matter EoS involves approximation schemes and includes adjustable parameters that are not really constrained by nuclear structure data. The resulting bulk properties of infinite nuclear matter (saturation density, binding energy, compression modulus, asymmetry energy) do not determine uniquely the parameters of nuclear energy density functionals, which usually must be further fine-tuned to ground-state data (masses and/or charge radii) of spherical nuclei.

In a phenomenological construction of a relativistic energy density functional one starts from an assumed ansatz for the medium dependence of the mean-field nucleon self-energies, and adjusts the free parameters directly to ground-states data of finite nuclei. This procedure was used, for instance, in the construction of the relativistic density-dependent interactions TW-99 [26], DD-ME1 [27], DD-ME2 [28], PKDD [40], PK01 [41], DD-PC1 [34].

3. Adjusting parameters to masses: the empirical functional DD-PC1

In an analysis of relativistic nuclear dynamics [42], modern high-precision nucleon–nucleon (NN) potentials (Argonne V_{18}, Bonn A, CD-Bonn, Idaho, Nijmegen, $V_{\mathrm{low}-k}$) were mapped on a relativistic operator basis, and the corresponding relativistic nucleon self-energies in nuclear matter were calculated in Hartree–Fock approximation at *tree level* [43]. A very interesting result is that, at moderate nucleon densities relevant for nuclear structure calculations, all potentials yield very similar scalar and vector mean fields of several hundred MeV magnitude, in remarkable agreement with standard RMF phenomenology: at saturation density a large and attractive scalar field $\Sigma_s \approx -400$ MeV, and a repulsive vector

field $\Sigma_v \approx 350$ MeV. The different treatment of short-distance dynamics in the various NN potentials leads to slightly more pronounced differences between the corresponding self-energies at higher nucleon densities. Generally, however, all potentials predict a very similar density dependence of the scalar and vector self-energies. In the chiral effective field theory framework, in particular, these self-energies are predominantly generated by contact terms that occur at next-to-leading order in the chiral expansion.

Of course at the Hartree–Fock level these NN potentials do not yield saturation of nuclear matter. Nevertheless, the corresponding self-energies can be used as the starting point in the modeling of medium dependence of a relativistic nuclear energy density functional. The density functional DD-PC1 [34], which is representative of the class of semi-empirical REDFs and will be used in illustrative calculations throughout this work, was adjusted starting from the Hartree–Fock isoscalar scalar and vector self-energies of the Idaho N^3LO potential [44]. The strength and density dependence of the interaction terms of the Lagrangian equation (8) were parameterized by the following ansatz:

$$\alpha_S(\rho) = a_S + (b_S + c_S x)\mathrm{e}^{-d_S x}, \tag{18}$$

$$\alpha_V(\rho) = a_V + b_V \mathrm{e}^{-d_V x}, \tag{19}$$

where $x = \rho/\rho_{\mathrm{sat}}$, and ρ_{sat} denotes the nucleon density at saturation in symmetric nuclear matter. In the isovector channel the corresponding Hartree–Fock nucleon self-energies, obtained by directly mapping microscopic NN potentials on a relativistic operator basis, are presently not available. Therefore, as it was done in the case of functionals based on finite-range meson-exchange interactions TW-99 [26], DD-ME1 [27], DD-ME2 [28], and PK01 [41], the density dependence of the isovector–vector coupling function was modeled based on the results of Dirac–Brueckner calculations of asymmetric nuclear matter [24]:

$$\alpha_{\mathrm{TV}}(\rho) = b_{\mathrm{TV}} \mathrm{e}^{-d_{\mathrm{TV}} x}. \tag{20}$$

The parameters of a nuclear EDF can be constrained by the choice of the nuclear matter (symmetric and asymmetric) equation of state. The functional DD-PC1 was eventually fine-tuned to experimental binding energies of finite nuclei and, since the calculated nuclear masses are not very sensitive to the nuclear matter saturation density, this quantity, together with the compression modulus and the Dirac mass, were kept fixed. The saturation density $\rho_{\mathrm{sat}} = 0.152$ fm^{-3} is in accordance with values predicted by most modern relativistic functionals, such as DD-ME1 [27], and DD-ME2 [28]. From these functionals also the Dirac effective nucleon mass was taken: $m_D^* = m + \Sigma_S = 0.58m$. The Dirac mass is closely related to the effective spin–orbit single-nucleon potential, and empirical energy spacings between spin–orbit partner states in finite nuclei determine a relatively narrow interval of allowed values: $0.57 \leq m_D^*/m \leq 0.61$. In Ref. [35] it was shown that, to reproduce experimental excitation energies of isoscalar giant monopole resonances, point-coupling interactions require a nuclear matter compression modulus close to 230 MeV, and thus $K_\infty = 230$ MeV was used for DD-PC1. Nuclear structure data do not constrain the nuclear matter EoS at high nucleon densities. Therefore, in addition to ρ_{sat}, m_D^*, and K_∞, two additional points on the $E(\rho)$ curve in symmetric matter were fixed to the microscopic EoS of Akmal et al. [45], based on the Argonne V_{18} NN potential and the UIX three-nucleon interaction. This EoS has extensively been used in studies of high-density nucleon matter and neutron stars.

The isovector channel of the energy density functional determines the density dependence of the nuclear matter symmetry energy

$$S_2(\rho) = a_4 + \frac{p_0}{\rho_{\mathrm{sat}}^2}(\rho - \rho_{\mathrm{sat}}) + \frac{\Delta K_0}{18\rho_{\mathrm{sat}}^2}(\rho - \rho_{\mathrm{sat}})^2 + \cdots. \tag{21}$$

The parameter p_0 characterizes the linear density dependence of the symmetry energy, and ΔK_0 is the isovector correction to the compression modulus. Experimental masses, unfortunately, do not place very strict constraints on the parameters of the expansion of $S_2(\rho)$ [46], but self-consistent mean-field calculations show that binding energies can restrict the values of S_2 at nucleon densities somewhat below saturation density, i.e. at $\rho \approx 0.1$ fm^{-3}. Additional information on the symmetry energy can be obtained from data on neutron skin thickness and excitation energies of giant dipole resonances. Although values of neutron radii are available only for a small number of nuclei and the corresponding uncertainties are large, recent studies have shown that relativistic effective interactions with volume asymmetry a_4 in the range 31 MeV $\leq a_4 \leq$ 35 MeV predict values for neutron skin thickness that are consistent with data, and reproduce experimental excitation energies of isovector giant dipole resonances (cf. Ref. [47] and references therein). For DD-PC1, therefore, the volume asymmetry was fixed at $a_4 = 33$ MeV, and the symmetry energy was varied at a density that corresponds to an average nucleon density in finite nuclei: $\langle\rho\rangle = 0.12$ fm^{-3}.

Until recently the standard procedure of fine-tuning non-relativistic or relativistic nuclear density functionals, was to perform a *least-squares* adjustment of a given set of free parameters simultaneously to a favorite nuclear matter EoS and to ground-state properties of about ten to twelve spherical closed-shell nuclei. Deformed systems have generally not been included in the adjustment of parameters because calculation of deformed nuclei is computationally much more intensive, especially in a multi-parameter fit. Ground-state data of closed-shell nuclei, however, include long-range correlations that cannot be absorbed into global functionals, e.g. correlations determined by the coupling to low-energy collective vibrations. The excitation energies and the structure of low-lying collective vibrational modes crucially depend on the details of single-nucleon levels in the vicinity of the Fermi surface and, therefore, the corresponding ground-state correlations obviously

cannot display a smooth dependence on nucleon number. On the other hand, it is well known that energy density functionals or, at the level of practical application, self-consistent mean-field models provide a much better description of deformed, open-shell nuclei. The reason is that the mean-field approach includes the mechanism of spontaneous symmetry breaking that generates the most important ground-state correlations in deformed nuclei: quadrupole correlations in the *ph*-channel and monopole-correlations in the *pp*-channel [2,48]. Additional rotational corrections that arise from the restoration of rotational symmetry vary rather smoothly over large mass intervals, and therefore can be included implicitly in the density functional. The same reasoning applies to corrections originating from the restoration of particle number in the regime of strong pairing realized in well-deformed nuclei. It also appears that those features of an effective interaction that determine surface properties are better constrained by binding energies of deformed systems, as compared to spherical nuclei [49]. The functional DD-PC1 was directly adjusted to binding energies of axially symmetric deformed nuclei in the mass regions $A \approx 150$–180 and $A \approx 230$–250. Similar approaches, employing data on both spherical and deformed nuclei, have recently been adopted in the optimization of nuclear energy density functionals of Skyrme type [49–51].

Calculated masses of finite nuclei are primarily sensitive to the three leading terms in the empirical mass formula: volume, surface and symmetry energy

$$\text{B.E.} = a_v A + a_s A^{2/3} + a_4 \frac{(N-Z)^2}{4A} + \cdots, \tag{22}$$

where a_v, a_s and a_4 correspond to the volume binding energy, surface energy, and symmetry energy, respectively, at saturation density in nuclear matter. One can, therefore, generate families of effective interactions that are characterized by different values of a_v, a_s and a_4 (or symmetry energy at a lower density, as explained above), and determine which parametrization minimizes the deviation from the empirical binding energies. Of course, if a functional is adjusted by varying the volume, symmetry, and surface energies, the parameters that determine these quantities will generally be correlated because of Eq. (22). When only a small number of nuclei is considered, satisfactory results can be obtained with various, in general linearly dependent combinations of parameters. The parameters of the functional DD-PC1 were thus determined in a careful comparison of the predicted binding energies with data, for a set of 64 nuclei with $A \approx 150$–180 and $A \approx 230$–250.

The ground states of 64 axially deformed nuclei were calculated in the self-consistent mean field approximation. Pairing correlations were treated in the BCS constant-gap approximation with empirical pairing gaps (5-point formula), and the pairing model space included two major oscillator shells ($2\hbar\omega_0$) above the Fermi surface. This approximation is justified because pairing correlations contribute only a very small portion to the total binding energy. In nuclei there is a clear separation of scales between the bulk contributions to the binding energies of the order of hundreds to more than thousand MeV, and the pairing energy of the order of ten MeV. To take into account pairing correlations in a calculation of the binding of nuclei close to β-stability, therefore, it is sufficient to consider only the monopole part of the effective pairing interaction adjusted to experimental paring gaps. This is, of course, no longer true in studies of phenomena determined by structure effects in the vicinity of the Fermi surface, such as nuclear excitations or fission barriers, or in nuclei far from stability, where detailed properties of the effective interaction in the pairing channel become important. In this review we will also present examples with more realistic pairing interactions, e.g. a zero-range force or a separable version of the Gogny force.

A careful analysis of deviations between calculated and experimental masses (mass residuals), showed a pronounced isospin and mass dependence of the residuals on the nuclear matter volume energy at saturation. To reduce the absolute mass residuals to less than 1 MeV, and to contain their mass and isotopic dependence, strict constraints on the value of a_v must be met. The narrow window of allowed values of the volume energy cannot be determined microscopically already at the nuclear matter level, but rather results from a fine-tuning of the parameters of the energy density functional to experimental masses. Calculated binding energies and charge radii are also sensitive to the choice of the surface coefficient a_s that determines the surface energy and surface thickness of semi-infinite nuclear matter. For the optimal density functional DD-PC1, characterized by the following properties at the saturation point: nucleon density $\rho_{\text{sat}} = 0.152$ fm^{-3}, volume energy $a_v = -16.06$ MeV, surface energy $a_s = 17.498$ MeV, symmetry energy $a_4 = 33$ MeV, and the nuclear matter compression modulus $K_{nm} = 230$ MeV, in Fig. 1 we display the absolute deviations of the calculated binding energies from the experimental values as functions of the isospin asymmetry

$$\alpha^2 = \frac{(N-Z)^2}{A^2},$$

and nucleon number. Positive deviations correspond to under-bound nuclei. The functional DD-PC1 corresponds to the lowest χ^2 value in the multi-parameter fit, and does not display any visible isotopic or mass dependence of the deviations of calculated masses. The absolute errors for all 64 axially deformed nuclei in the mass regions $A \approx 150$–180 and $A \approx 230$–250 are smaller than 1 MeV. With stronger binding in symmetric nuclear matter (i.e. by increasing the absolute value of a_v), the corresponding deviations of calculated binding energies become larger, and they also acquire a definite isotopic dependence. Reducing the absolute value of a_v reverses the isotopic trend of the errors.

The density functional DD-PC1 has been further tested in calculations of properties of spherical and deformed medium-heavy and heavy nuclei, including binding energies, charge radii, deformation parameters, neutron skin thickness, and excitation energies of giant multipole resonances. Results have been compared with available data, and with predictions of the most successful finite-range meson-exchange relativistic effective interactions. In general, a very good agreement with data has been obtained except, perhaps, for the effect of overbinding of spherical closed-shell nuclei. DD-PC1, like virtually

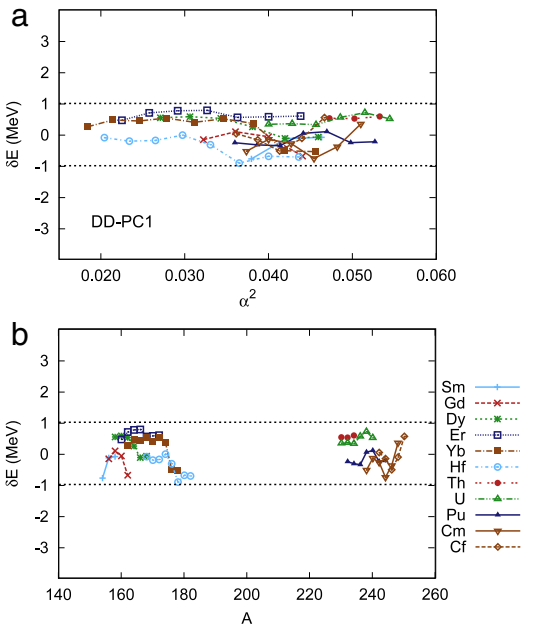

Fig. 1. Absolute deviations of the calculated binding energies from the experimental values of the 64 axially deformed nuclei, as functions of the asymmetry coefficient (upper panel), and mass number (lower panel). Lines connect nuclei that belong to the isotopic chains shown in the legend. The theoretical binding energies are calculated using the relativistic density functional DD-PC1.

all relativistic mean-field models, is characterized by a relatively low effective nucleon mass and, when adjusted to masses of deformed nuclei, it overbinds spherical closed-shell systems. The well known problem of "arches" of mass residuals between shell closures could, in principle, be addressed by a functional that goes beyond the static mean-field approximation and includes an explicit energy dependence of the nucleon self-energies. Very good results have been obtained for the excitation energies of giant monopole and dipole resonances in spherical nuclei, calculated using the relativistic quasiparticle random-phase approximation based on the DD-PC1 functional. The agreement with data validates the choice of the nuclear matter compressibility and symmetry energy for DD-PC1. The total number of parameters is 10, similar to most non-relativistic Skyrme-type density functionals. The effective Lagrangian of DD-PC1 contains only four interaction terms except, of course, the Coulomb term (cf. Eq. (8)), and the 10 parameters determine the density dependence of the strength functionals and reflect the complex nuclear many-body dynamics.

In the following sections we will also employ DD-PC1 in a series of spectroscopic calculations utilizing models that go beyond the "mean-field" level, and explicitly include collective correlations related to restoration of broken symmetries and fluctuations in quadrupole coordinates. Strictly speaking, those correlations that are treated explicitly should not be included in the density functional in an implicit way, that is, in the parameters adjusted to data that already include correlations. In future studies the solution could be to adjust the functional to pseudodata, obtained by subtracting correlation effects from experimental masses and, eventually, radii. In deformed nuclei the dominant contribution to ground-state correlations is the rotational energy correction [52], which is relatively simple to calculate. Approximate methods have been developed that enable a systematic evaluation of correlation energies for the nuclear mass table [53]. Starting from a set of pseudodata, one expects that the corresponding modifications of the parameters of the energy density functional will be relatively small. However, even a small change in the relative contribution of various interaction terms could be the decisive factor in specific cases of soft potential energy surfaces, coexistence of prolate and oblate shapes, level ordering, etc.

4. 3D relativistic Hartree–Bogoliubov model with a separable pairing interaction

Relativistic energy density functionals have been employed in analyses of properties of ground and excited states in spherical and deformed nuclei. For a quantitative analysis of open-shell nuclei it is necessary to consider also pairing correlations. Pairing has often been taken into account in a very phenomenological way in the BCS model with the monopole pairing force, adjusted to the experimental odd–even mass differences. In many cases, however, this approach presents only a poor approximation. The physics of weakly-bound nuclei, in particular, necessitates a unified and self-consistent treatment of mean-field and pairing correlations. This has led to the formulation and development of the relativistic Hartree–Bogoliubov (RHB) model [54], which represents a relativistic extension of the conventional Hartree–Fock–Bogoliubov framework. The RHB model provides a unified description of particle–hole (*ph*) and particle–particle (*pp*) correlations on a mean-field level by using two average potentials: the self-consistent mean field that encloses all the long range *ph* correlations, and a pairing field $\hat{\Delta}$ which sums up the *pp*-correlations. The ground state of a nucleus is described by a generalized Slater determinant

$|\Phi\rangle$ that represents the vacuum with respect to independent quasiparticles. The quasiparticle operators are defined by the unitary Bogoliubov transformation of the single-nucleon creation and annihilation operators:

$$\alpha_k^+ = \sum_l U_{lk} c_l^+ + V_{lk} c_l, \tag{23}$$

where U and V are the Hartree–Bogoliubov wave functions determined by the solution of the RHB equation. In coordinate representation:

$$\begin{pmatrix} h_D - m - \lambda & \Delta \\ -\Delta^* & -h_D^* + m + \lambda \end{pmatrix} \begin{pmatrix} U_k(\boldsymbol{r}) \\ V_k(\boldsymbol{r}) \end{pmatrix} = E_k \begin{pmatrix} U_k(\boldsymbol{r}) \\ V_k(\boldsymbol{r}) \end{pmatrix}. \tag{24}$$

In the relativistic case the self-consistent mean-field corresponds to the single-nucleon Dirac Hamiltonian $\hat{h}_D$ of Eq. (10). m is the nucleon mass, and the chemical potential λ is determined by the particle number subsidiary condition such that the expectation value of the particle number operator in the ground state equals the number of nucleons. The pairing field Δ reads

$$\Delta_{ab}(\boldsymbol{r}, \boldsymbol{r}') = \frac{1}{2} \sum_{c,d} V_{abcd}(\boldsymbol{r}, \boldsymbol{r}') \kappa_{cd}(\boldsymbol{r}, \boldsymbol{r}') \tag{25}$$

where $V_{abcd}(\boldsymbol{r}, \boldsymbol{r}')$ are the matrix elements of the two-body pairing interaction, and the indices a, b, c and d denote the quantum numbers that specify the Dirac indices of the spinor. The column vectors denote the quasiparticle wave functions, and E_k are the quasiparticle energies. The dimension of the RHB matrix equation is two times the dimension of the corresponding Dirac equation. For each eigenvector (U_k, V_k) with positive quasiparticle energy $E_k > 0$, there exists an eigenvector (V_k^*, U_k^*) with quasiparticle energy $-E_k$. Since the baryon quasiparticle operators satisfy fermion commutation relations, the levels E_k and $-E_k$ cannot be occupied simultaneously. For the solution that corresponds to a ground state of a nucleus with even particle number, one usually chooses the eigenvectors with positive eigenvalues E_k.

The single-particle density and the pairing tensor, constructed from the quasi-particle wave functions

$$\rho_{cd}(\boldsymbol{r}, \boldsymbol{r}') = \sum_{k>0} V_{ck}^*(\boldsymbol{r}) V_{dk}(\boldsymbol{r}'), \tag{26}$$

$$\kappa_{cd}(\boldsymbol{r}, \boldsymbol{r}') = \sum_{k>0} U_{ck}^*(\boldsymbol{r}) V_{dk}(\boldsymbol{r}'), \tag{27}$$

are calculated in the *no-sea* approximation (denoted by $k > 0$): the summation runs over all quasiparticle states k with positive quasiparticle energies $E_k > 0$, but omits states that originate from the Dirac sea. The latter are characterized by quasiparticle energies larger than the Dirac gap ($\approx$1200 MeV).

Pairing correlations in nuclei are restricted to an energy window of a few MeV around the Fermi level, and their scale is well separated from the scale of binding energies, which are in the range of several hundred to thousand MeV. There is no empirical evidence for any relativistic effect in the nuclear pairing field $\hat{\Delta}$ and, therefore, a hybrid RHB model with a non-relativistic pairing interaction can be employed. For a general two-body interaction, the matrix elements of the relativistic pairing field read

$$\hat{\Delta}_{a_1 p_1, a_2 p_2} = \frac{1}{2} \sum_{a_3 p_3, a_4 p_4} \langle a_1 p_1, a_2 p_2 | V^{pp} | a_3 p_3, a_4 p_4 \rangle_a \kappa_{a_3 p_3, a_4 p_4}, \tag{28}$$

where the indices $(p_1, p_2, p_3, p_4 \equiv f, g)$ refer to the large and small components of the quasiparticle Dirac spinors:

$$U(\mathbf{r}, s, t) = \begin{pmatrix} f_U(\mathbf{r}, s, t) \\ \mathrm{i} g_U(\mathbf{r}, s, t) \end{pmatrix} \qquad V(\mathbf{r}, s, t) = \begin{pmatrix} f_V(\mathbf{r}, s, t) \\ \mathrm{i} g_V(\mathbf{r}, s, t) \end{pmatrix}. \tag{29}$$

In practical applications of the RHB model to finite open-shell nuclei, only the large components of the spinors $U_k(\mathbf{r})$ and $V_k(\mathbf{r})$ are used to build the non-relativistic pairing tensor $\hat{\kappa}$ in Eq. (26). The resulting pairing field reads

$$\hat{\Delta}_{a_1 f, a_2 f} = \frac{1}{2} \sum_{a_3 f, a_4 f} \langle a_1 f, a_2 f | V^{pp} | a_3 f, a_4 f \rangle_a \kappa_{a_3 f, a_4 f}. \tag{30}$$

The other components: $\hat{\Delta}_{fg}$, $\hat{\Delta}_{gf}$, and $\hat{\Delta}_{gg}$ can be safely omitted [55].

In most applications of the RHB model [12] the pairing part of the Gogny force [56] has been employed in the particle–particle (pp) channel:

$$V^{pp}(1,2) = \sum_{i=1,2} \mathrm{e}^{-((\mathbf{r}_1 - \mathbf{r}_2)/\mu_i)^2} (W_i + B_i P^\sigma - H_i P^\tau - M_i P^\sigma P^\tau), \tag{31}$$

with the set D1S [57] for the parameters μ_i, W_i, B_i, H_i, and M_i ($i = 1, 2$). A basic advantage of the Gogny force is the finite range, which automatically guarantees a proper cut-off in momentum space. However, the resulting pairing field is non-local

and the solution of the corresponding Dirac–Hartree–Bogoliubov integro-differential equations can be time-consuming, especially in the case 3D calculations for nuclei with triaxial shapes.

In a series of recent articles [58–61] a separable form of the pairing force has been introduced for RHB calculations in spherical and deformed nuclei. The force is separable in momentum space, and is completely determined by two parameters that are adjusted to reproduce in symmetric nuclear matter the bell-shape curve of the pairing gap of the Gogny force. The gap equation in the $^1S_0$ channel reads

$$\Delta(k) = -\int_0^\infty \frac{k'^2 \mathrm{d}k'}{2\pi^2} \langle k|V^{^1S_0}|k'\rangle \frac{\Delta(k')}{2E(k')}, \tag{32}$$

and the pairing force is separable in momentum space:

$$\langle k|V^{^1S_0}|k'\rangle = -Gp(k)p(k'). \tag{33}$$

By assuming a simple Gaussian ansatz $p(k) = \mathrm{e}^{-a^2k^2}$, the two parameters G and a have been adjusted to reproduce the density dependence of the gap at the Fermi surface, calculated with a Gogny force. For the D1S parameterization [57] of the Gogny force the following values were determined: $G = -728$ MeV fm^3 and $a = 0.644$ fm. When the pairing force Eq. (33) is transformed from momentum to coordinate space, it takes the form:

$$V(\boldsymbol{r}_1, \boldsymbol{r}_2, \boldsymbol{r}_1', \boldsymbol{r}_2') = G\delta\left(\boldsymbol{R} - \boldsymbol{R}'\right) P(\boldsymbol{r}) P(\boldsymbol{r}') \frac{1}{2}\left(1 - P^\sigma\right), \tag{34}$$

where $\boldsymbol{R} = \frac{1}{2}(\boldsymbol{r}_1 + \boldsymbol{r}_2)$ and $\boldsymbol{r} = \boldsymbol{r}_1 - \boldsymbol{r}_2$ denote the center-of-mass and the relative coordinates, and $P(\boldsymbol{r})$ is the Fourier transform of $p(k)$:

$$P(\boldsymbol{r}) = \frac{1}{\left(4\pi a^2\right)^{3/2}} \mathrm{e}^{-\boldsymbol{r}^2/4a^2}. \tag{35}$$

The pairing force has finite range and, because of the presence of the factor $\delta\left(\boldsymbol{R} - \boldsymbol{R}'\right)$, it preserves translational invariance. Even though $\delta\left(\boldsymbol{R} - \boldsymbol{R}'\right)$ implies that this force is not completely separable in coordinate space, the corresponding anti-symmetrized pp matrix elements

$$\langle \alpha\bar{\beta}|V|\gamma\bar{\delta}\rangle_a = \langle \alpha\bar{\beta}|V|\gamma\bar{\delta}\rangle - \langle \alpha\bar{\beta}|V|\bar{\delta}\gamma\rangle, \tag{36}$$

can be represented as a sum of a finite number of separable terms in the basis of a 3D harmonic oscillator.

The Dirac–Hartree–Bogoliubov equations (24) are solved by expanding the nucleon spinors in the basis of a 3D harmonic oscillator in Cartesian coordinates [61]. In this way both axial and triaxial nuclear shapes can be described. To obtain complete convergence, for medium heavy nuclei the basis must include at least $N_f^{\max} = 14$ major oscillator shells, and for very heavy nuclei $N_f^{\max} = 16$ major oscillator shells are necessary. The map of the energy surface as a function of the quadrupole deformation is obtained by imposing constraints on the axial and triaxial quadrupole moments. The method of quadratic constraints uses an unrestricted variation of the function

$$\langle \hat{H}\rangle + \sum_{\mu=0,2} C_{2\mu}\left(\langle \hat{Q}_{2\mu}\rangle - q_{2\mu}\right)^2, \tag{37}$$

where $\langle \hat{H}\rangle$ is the total energy, and $\langle \hat{Q}_{2\mu}\rangle$ denotes the expectation value of the mass quadrupole operators:

$$\hat{Q}_{20} = 2z^2 - x^2 - y^2 \quad \text{and} \quad \hat{Q}_{22} = x^2 - y^2. \tag{38}$$

$q_{2\mu}$ is the constrained value of the multipole moment, and $C_{2\mu}$ the corresponding stiffness constant [62]. For a self-consistent solution the quadratic constraint adds an extra force $\sum_{\mu=0,2} \lambda_\mu \hat{Q}_{2\mu}$ to the system, where $\lambda_\mu = 2C_{2\mu}(\langle \hat{Q}_{2\mu}\rangle - q_{2\mu})$. Such a force is necessary to keep the system at a point different from a stationary point. In general, the values of the quadrupole moments $\langle \hat{Q}_{2\mu}\rangle$ of the self-consistent solution coincide with the constrained values $q_{2\mu}$ only at the stationary points. Moreover, the difference between the quadrupole moment $\langle \hat{Q}_{2\mu}\rangle$ and the constrained value $q_{2\mu}$ depends on the value of the stiffness constant, that is, smaller values of $C_{2\mu}$ lead to larger deviations of the quadrupole moment from the corresponding constrained value. Increasing the value of the stiffness constant, however, often destroys the convergence of the self-consistent procedure. This deficiency can be resolved by implementing the augmented Lagrangian method [63], and this approach has been used in all constrained calculations presented in this work.

Figs. 2 and 3 display the results of self-consistent 3D RHB calculations for the isotopic chains of Th, U, Pu, Cm, Cf, Fm, and No. The absolute deviations of the calculated binding energies from data [64] (Fig. 2) show an excellent agreement between theory and experiment. Except for the isotopes of No, all the calculated nuclei are slightly underbound, but the absolute differences between calculated and experimental binding energies is less than 1 MeV in all cases. The calculated ground-state quadrupole Q_{20}, and hexadecapole Q_{40}, moments are compared with available data [65] in Fig. 3. We notice that the

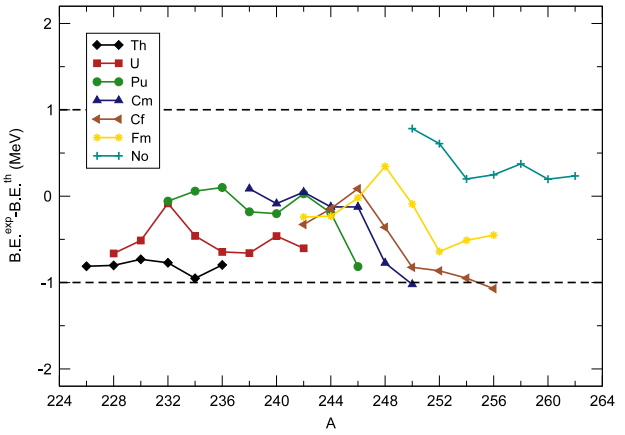

Fig. 2. Absolute deviations of the calculated relativistic Hartree–Bogoliubov (RHB) binding energies from the experimental values [64], for the isotopic chains of Th, U, Pu, Cm, Cf, Fm, and No.

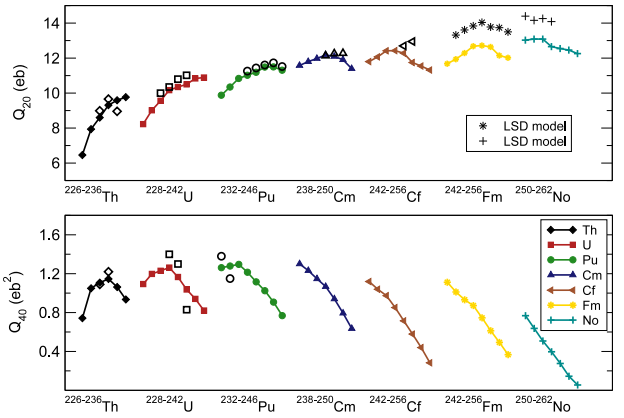

Fig. 3. Self-consistent RHB ground-state axial quadrupole and hexadecapole moments in comparison with data [65] (open symbols), for the isotopic chains of Th, U, Pu, Cm, Cf, Fm, and No. For Fm and No the calculated quadrupole moments are compared with values predicted by the LSD model [66].

values predicted by the DD-PC1 functional reproduce in detail the isotopic trend of the empirical moments in the Th, U, Pu and Cm sequences, and are in very good agreement with the quadrupole moments of the Cf isotopes. No data on ground-state moments are available for the isotopes of Fm and No. The calculated 3D RHB quadrupole moments are compared with values estimated in axially-symmetric calculations with the Lublin–Strasburg drop (LSD) model [66].

The structure of the nucleus ^{240}Pu and its double-humped fission barrier has become a standard benchmark for models based on the self-consistent mean-field approach and the corresponding effective interactions or density functionals. In Fig. 4 we display the RHB triaxial quadrupole binding energy map of ^{240}Pu in the $\beta - \gamma$ plane ($0 \leq \gamma \leq 60^\circ$), calculated with the DD-PC1 energy density functional plus the pairing interaction Eq. (34) [67]. The calculation has been carried out on a mesh of quadrupole deformation parameters with $\Delta\beta = 0.05$ and $\Delta\gamma = 6^\circ$. All energies are normalized with respect to the binding energy of the absolute minimum, and the color code refers to the energy of each point on the surface relative to the minimum. Since the present implementation of the model does not include reflection asymmetric shapes, the potential energy surface (PES) is calculated only up to $\beta \leq 1.3$. For larger deformations, i.e. in the region of the second barrier, octupole deformations should be taken into account. The absolute minimum is calculated at $\beta = 0.28$, $\gamma = 0^\circ$, and a second (super-deformed) valley is predicted around $\beta \approx 0.9$. The axially symmetric barrier at $\beta \approx 0.5$ is bypassed through the triaxial region, bringing the height of the barrier much closer to the empirical value. This is shown more clearly in Fig. 5, where we plot the deformation energy curves and the inner barrier of ^{240}Pu as functions of the axial deformation β. The two curves correspond to the axially-symmetric RHB calculation (solid), and to the projection on the β-axis of the triaxial PES (dashed). The experimental values for the ground-state deformation, the barrier height, and the energy of the second minimum are taken from Refs. [68–71]. One might notice a very good agreement between theory and available data. In particular, the inclusion of triaxial shapes lowers the inner barrier by ≈2 MeV. Similar results have also been obtained in constrained self-consistent mean-field calculations using Skyrme functionals [2], and in the HFB + Gogny analysis of the actinide region [72] it was shown that the inner barriers of the actinides are systematically lowered by up to 4 MeV when calculations included triaxial shapes.

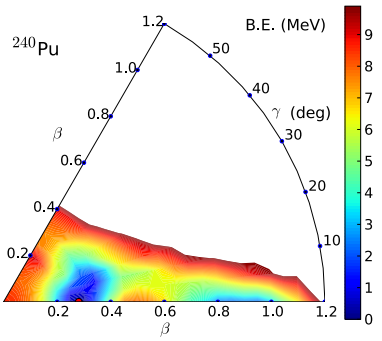

Fig. 4. Self-consistent RHB triaxial quadrupole binding energy maps of ^{240}Pu in the $\beta - \gamma$ plane ($0 \leq \gamma \leq 60^{\circ}$). All energies are normalized with respect to the binding energy of the absolute minimum. The color code refers to the energy of each point on the surface relative to the minimum.

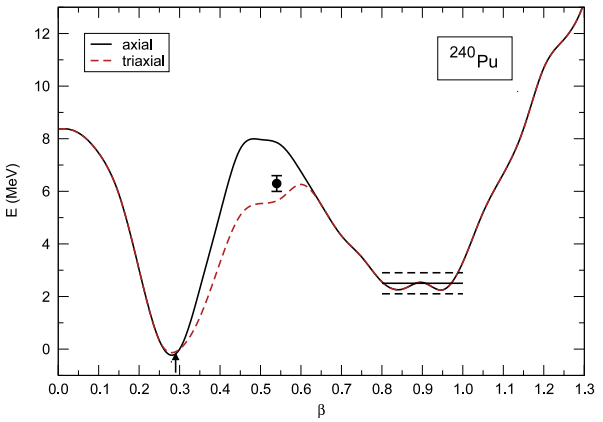

Fig. 5. (Color online) Deformation energy curves and the inner barrier of ^{240}Pu as functions of the axial deformation β. The two curves correspond to the axially-symmetric RHB calculation (solid), and to the projection on the β-axis of the triaxial PES (dashed), calculated with the functional DD-PC1. The experimental values for the ground-state deformation, the barrier height, and the energy of the second minimum are indicated, respectively, with an arrow, a symbol with error bars and three lines indicating the value and its errors.
Source: The data are taken from Refs. [68–71].

The 3D relativistic Hartree–Bogoliubov model, with the functional DD-PC1 in the particle–hole channel and a separable pairing force in the particle–particle channel, enables very efficient constrained self-consistent triaxial calculations of binding energy maps as functions of quadrupole deformation in the $\beta - \gamma$ plane. The resulting single-quasiparticle energies and wave functions can be employed as microscopic input for the generator coordinate method configuration mixing of angular-momentum projected triaxial wave functions, or can be used to determine the parameters of the collective Hamiltonian for vibrations and rotations: the mass parameters, the moments of inertia, and the collective potential. The solution of the corresponding eigenvalue problem yields the excitation spectra and collective wave functions that are used in the calculation of electromagnetic transition probabilities. This approach will be illustrated in the next two sections.

5. Beyond the mean-field approximation: restoring broken symmetries and configuration mixing calculations

Nuclear structure far from stability has become a subject of extensive experimental and theoretical studies. The variation of ground-state shapes in an isotopic chain, for instance, is governed by the evolution of shell structure. Far from the β-stability line, in particular, the energy spacings between single-particle levels change considerably with the number of neutrons and/or protons. This can result in reduced spherical shell gaps, modifications of shell structure, and in some cases spherical magic numbers may disappear. The reduction of a spherical shell closure is associated with the occurrence of deformed ground states and, in a number of cases, with the phenomenon of shape coexistence.

A quantitative description of structure phenomena related to shell evolution necessitates the inclusion of many-body correlations beyond the mean-field approximation. The starting point is usually a constrained Hartree–Fock plus BCS (HF-BCS), or Hartree–Fock–Bogoliubov (HFB) calculation of the potential energy surface with the mass quadrupole components as constrained quantities. When based on microscopic EDFs or effective interactions, such calculations comprise short- and long-range many-body correlations, and result in static symmetry-breaking product many-body states. Static mean-field models provide a description of bulk properties, such as masses and radii. To calculate energy spectra and transition probabilities, however, it is essential to include collective correlations that arise from symmetry restoration and fluctuations

around the mean-field minimum. Because they are susceptible to shell effects and vary with nucleon number, collective correlations cannot be be incorporated in a universal EDF. In deformed nuclei, for instance, the rotational energy correction, that is, the energy gained by the restoration of rotational symmetry, is proportional to the quadrupole deformation of the symmetry-breaking state and can reach several MeV for a well deformed configuration. Fluctuations of quadrupole deformation also contribute to the correlation energy. Both types of correlations can be included simultaneously by mixing angular-momentum projected states corresponding to different quadrupole moments. The most effective approach for configuration mixing calculations is the generator coordinate method (GCM), with multipole moments used as coordinates that generate the intrinsic wave functions.

In recent years several accurate and efficient models and algorithms, based on microscopic density functionals or effective interactions, have been developed that perform the restoration of symmetries broken by the static nuclear mean field, and take into account quadrupole fluctuations. Many interesting phenomena related to shell evolution have been investigated by employing the angular-momentum projected GCM with the axial quadrupole moment as the generating coordinate, and with intrinsic configurations calculated in the HFB model with the finite-range Gogny interaction [73–77]. Very recently this approach has been extended to include full triaxial angular-momentum and particle-number projection [78]. Another sophisticated structure model that takes into account collective correlations is based on axially constrained HF + BCS calculations with Skyrme effective interactions in the particle–hole channel and a density-dependent contact force in the pairing channel [79–83]. Particle numbers and rotational symmetry are restored by projecting self-consistent mean-field wave functions on the correct numbers of neutrons and protons, and on angular momentum. Finally, a mixing of the projected wave functions corresponding to different quadrupole moments is performed with a discretized version of the generator coordinate method. The latest extension of this model that incorporates triaxial angular-momentum projection was reported in Ref. [84].

In a series of recent articles we have expanded the framework of relativistic energy density functionals to include correlations related to the restoration of broken symmetries and to fluctuations of collective variables. A model has been developed that uses the GCM to perform configuration mixing of angular-momentum [15], and also particle-number projected [16] relativistic wave functions. The geometry was restricted to axially symmetric shapes, and the intrinsic wave functions were generated from solutions of the relativistic mean-field + Lipkin–Nogami BCS equations, with a constraint on the mass quadrupole moment. In the first application [85], the GCM based on relativistic EDFs was employed in a study of shape transitions in Nd isotopes. This approach has been further developed in Refs. [18,19] by implementing a model that includes triaxial angular-momentum projection.

Here we will illustrate the "beyond mean-field" extension of the relativistic EDF approach by considering a rather simple example of a GCM configuration mixing of angular-momentum projected wave functions, generated from the self-consistent solutions of axially symmetric constrained RMF+BCS equations for ^{154}Sm.

5.1. GCM mixing of angular-momentum projected states

The generator coordinate method (GCM) is based on the assumption that, starting from a set of intrinsic symmetry-breaking states $|\phi(q)\rangle$ which depend on a collective coordinate q, one can build approximate eigenstates of the nuclear Hamiltonian [62]

$$|\Psi_\alpha\rangle = \sum_j f_\alpha(q_j)|\phi(q_j)\rangle. \tag{39}$$

Here the basis states $|\phi(q)\rangle$ are Slater determinants of single-nucleon states generated by solving the constrained relativistic mean-field + BCS equations with the mass quadrupole moment as the generating coordinate q. The axially deformed mean-field breaks rotational symmetry, so that the basis states $|\phi(q)\rangle$ are not eigenstates of the total angular momentum. To be able to compare theoretical results with data, it is necessary to construct states with good angular momentum

$$|\Psi^{JM}_\alpha\rangle = \sum_{j,K} f^{JK}_\alpha(q_j)\hat{P}^J_{MK}|\phi(q_j)\rangle, \tag{40}$$

where $\hat{P}^J_{MK}$ denotes the angular momentum projection operator

$$\hat{P}^J_{MK} = \frac{2J+1}{8\pi^2}\int \mathrm{d}\Omega D^{J*}_{MK}(\Omega)\hat{R}(\Omega). \tag{41}$$

The integration is performed over the three Euler angles α, β, and γ. $D^J_{MK}(\Omega) = \mathrm{e}^{-\mathrm{i}M\alpha}d^J_{MK}(\beta)\mathrm{e}^{-\mathrm{i}K\gamma}$ is the Wigner function, and $\hat{R}(\Omega) = \mathrm{e}^{-\mathrm{i}\alpha\hat{J}_z}\mathrm{e}^{-\mathrm{i}\beta\hat{J}_y}\mathrm{e}^{-\mathrm{i}\gamma\hat{J}_z}$ is the rotation operator. The weight functions $f^{JK}_\alpha(q_j)$ are determined from the variation:

$$\delta E^J = \delta\frac{\langle\Psi^{JM}_\alpha|\hat{H}|\Psi^{JM}_\alpha\rangle}{\langle\Psi^{JM}_\alpha|\Psi^{JM}_\alpha\rangle} = 0, \tag{42}$$

that is, by requiring that the expectation value of the energy is stationary with respect to an arbitrary variation δf^{JK}_α. This leads to the Hill–Wheeler equation

$$\sum_{j,K} f_{\alpha}^{JK}(q_j)\left(\langle\phi(q_i)|\hat{H}\hat{P}^J_{MK}|\phi(q_j)\rangle - E^J_{\alpha}\langle\phi(q_i)|\hat{P}^J_{MK}|\phi(q_j)\rangle\right) = 0. \tag{43}$$

The restriction to axially symmetric configurations ($\hat{J}_z|\phi(q)\rangle = 0$) simplifies the problem considerably, because in this case the integrals over the Euler angles α and γ can be performed analytically, and for an arbitrary multipole operator $\hat{Q}_{\lambda\mu}$ one thus finds

$$\langle\phi(q_i)|\hat{Q}_{\lambda\mu}\hat{P}^J_{MK}|\phi(q_j)\rangle = (2J+1)\frac{1+(-1)^J}{2}\delta_{M-\mu}\delta_{K0}\int_0^{\pi/2}\mathrm{d}\beta\,\sin\beta d^{J*}_{-\mu 0}(\beta)\langle\phi(q_i)|\hat{Q}_{\lambda\mu}\mathrm{e}^{-\mathrm{i}\beta\hat{J}_y}|\phi(q_j)\rangle. \tag{44}$$

This expression vanishes for odd values of angular momentum J and, therefore, all projected quantities are defined only for even values of J. The norm overlap kernel

$$\begin{aligned}\mathcal{N}^J(q_i,q_j) &= \langle\phi(q_i)|\hat{P}^J_{MK}|\phi(q_j)\rangle \\ &= (2J+1)\frac{1+(-1)^J}{2}\delta_{M0}\delta_{K0}\int_0^{\pi/2}\mathrm{d}\beta\,\sin\beta d^{J*}_{00}(\beta)\langle\phi(q_i)|\mathrm{e}^{-\mathrm{i}\beta\hat{J}_y}|\phi(q_j)\rangle,\end{aligned} \tag{45}$$

can be evaluated by employing the generalized Wick theorem:

$$n(q_i,q_j;\beta) \equiv \langle\phi(q_i)|\mathrm{e}^{-\mathrm{i}\beta\hat{J}_y}|\phi(q_j)\rangle = \pm\sqrt{\det\mathcal{N}_{ab}(q_i,q_j;\beta)}. \tag{46}$$

The overlap matrix is defined as:

$$\mathcal{N}_{ab}(q_i,q_j;\beta) = u_a(q_i)R_{ab}(q_i,q_j;\beta)u_b(q_j) + v_a(q_i)R_{ab}(q_i,q_j;\beta)v_b(q_j), \tag{47}$$

where u and v denote the BCS occupation probabilities, the matrix R reads

$$R_{ab}(q_i,q_j;\beta) = \int\psi^{\dagger}_a(\boldsymbol{r};q_i)\mathrm{e}^{-\mathrm{i}\beta\hat{J}_y}\psi_b(\boldsymbol{r};q_j)\mathrm{d}\boldsymbol{r}, \tag{48}$$

and $\psi_a(\boldsymbol{r};q_i)$ denotes the self-consistent intrinsic single-nucleon spinor at the generating coordinate q_i. The Hamiltonian kernel

$$\begin{aligned}\mathcal{H}^J(q_i,q_j) &= \langle\phi(q_i)|\hat{H}\hat{P}^J_{MK}|\phi(q_j)\rangle \\ &= (2J+1)\frac{1+(-1)^J}{2}\delta_{M0}\delta_{K0}\int_0^{\pi/2}\mathrm{d}\beta\,\sin\beta d^{J*}_{00}(\beta)\langle\phi(q_i)|\hat{H}\mathrm{e}^{-\mathrm{i}\beta\hat{J}_y}|\phi(q_j)\rangle,\end{aligned} \tag{49}$$

can be calculated from the energy functional provided the *intrinsic* densities are replaced by *transition* one-body matrices when evaluating the expression

$$h(q_i,q_j;\beta) \equiv \langle\phi(q_i)|\hat{H}\mathrm{e}^{-\mathrm{i}\beta\hat{J}_y}|\phi(q_j)\rangle = \int\mathrm{d}\boldsymbol{r}\,\mathcal{E}_{tot}(\boldsymbol{r};q_i,q_j,\beta). \tag{50}$$

The basis states $|\phi(q_j)\rangle$ are not eigenstates of the proton and neutron number operators $\hat{Z}$ and $\hat{N}$. The adjustment of the Fermi energies in a BCS calculation ensures only that the average value of the nucleon number operators corresponds to the actual number of nucleons. Consequently, the wave functions $|\Psi^{JM}_{\alpha}\rangle$ are generally not eigenstates of the nucleon number operators and, moreover, the average values of the nucleon number operators are not necessarily equal to the number of nucleons in a given nucleus. To restore the correct mean values of the nucleon numbers, one can modify the Hill–Wheeler equation by replacing $h(q_i,q_j;\beta)$ with

$$h'(q_i,q_j;\beta) = h(q_i,q_j;\beta) - \lambda_p\left[z(q_i,q_j;\beta) - z_0\right] - \lambda_n\left[n(q_i,q_j;\beta) - n_0\right], \tag{51}$$

where

$$z(q_i,q_j;\beta) = \langle\phi(q_i)|\hat{Z}\mathrm{e}^{-\mathrm{i}\beta\hat{J}_y}|\phi(q_j)\rangle, \tag{52}$$

and

$$n(q_i,q_j;\beta) = \langle\phi(q_i)|\hat{N}\mathrm{e}^{-\mathrm{i}\beta\hat{J}_y}|\phi(q_j)\rangle. \tag{53}$$

$\lambda_{p(n)}$ is the proton (neutron) Fermi energy, while z_0 and n_0 denote the desired number of protons and neutrons, respectively.

The Hill–Wheeler equation

$$\sum_j\mathcal{H}^J(q_i,q_j)f^J_{\alpha}(q_j) = E^J_{\alpha}\sum_j\mathcal{N}^J(q_i,q_j)f^J_{\alpha}(q_j), \tag{54}$$

presents a generalized eigenvalue problem, and thus the weight functions $f^J_\alpha(q_i)$ are not orthogonal and cannot be interpreted as collective wave functions for the variable q. It is useful to re-express Eq. (54) in terms of another set of functions, $g^J_\alpha(q_i)$, defined by

$$g^J_\alpha(q_i) = \sum_j (\mathcal{N}^J)^{1/2}(q_i, q_j) f^J_\alpha(q_j). \tag{55}$$

With this transformation the Hill–Wheeler equation defines an ordinary eigenvalue problem

$$\sum_j \tilde{\mathcal{H}}^J(q_i, q_j) g^J_\alpha(q_j) = E_\alpha g^J_\alpha(q_i), \tag{56}$$

with

$$\tilde{\mathcal{H}}^J(q_i, q_j) = \sum_{k,l} (\mathcal{N}^J)^{-1/2}(q_i, q_k) \mathcal{H}^J(q_k, q_l) (\mathcal{N}^J)^{-1/2}(q_l, q_j). \tag{57}$$

The functions $g^J_\alpha(q_i)$ are orthonormal and play the role of collective wave functions.

Once the weight functions $f^J_\alpha(q)$ are known, it is straightforward to calculate all physical observables, such as transition probabilities and spectroscopic quadrupole moments. The reduced transition probability for a transition between an initial state (J_i, α_i), and a final state (J_f, α_f), reads

$$B(\mathrm{E2}; J_i\alpha_i \to J_f\alpha_f) = \frac{e^2}{2J_i+1} \left| \sum_{q_f, q_i} f^{J_f *}_{\alpha_f}(q_f) \langle J_f q_f || \hat{Q}_2 || J_i q_i \rangle f^{J_i}_{\alpha_i}(q_i) \right|^2. \tag{58}$$

5.2. Angular momentum projection and configuration mixing: ^{154}Sm

As an illustration of GCM configuration mixing of angular-momentum projected states, we consider the case of the prolate deformed, axially-symmetric ground state of ^{154}Sm. The intrinsic symmetry-breaking wave functions that are used in the configuration mixing calculation are obtained as solutions of the self-consistent relativistic mean-field equations, subject to constraint on the mass quadrupole moment. The interaction in the particle–hole channel is determined by the density functional DD-PC1, and a density-independent δ-force is used as the effective interaction in the particle–particle channel, supplemented with a smooth cut-off determined by a Fermi function in the single-particle energies [33]. Pairing correlations are treated within the BCS framework, and the pairing contribution to the total energy is given by

$$E^{p(n)}_{\mathrm{pair}} = \int \mathcal{E}^{p(n)}_{\mathrm{pair}}(\boldsymbol{r}) \mathrm{d}\boldsymbol{r} = \frac{V_{p(n)}}{4} \int \kappa^*_{p(n)}(\boldsymbol{r}) \kappa_{p(n)}(\boldsymbol{r}) \mathrm{d}\boldsymbol{r}, \tag{59}$$

for protons and neutrons, respectively. $\kappa_{p(n)}(\boldsymbol{r})$ denotes the local part of the pairing tensor, and $V_p = -321$ MeV fm^3 and $V_n = -308$ MeV fm^3 are the pairing strength parameters adjusted to empirical pairing gaps. We note that while the BCS constant-gap approximation was employed in the fit of the parameters of the functional DD-PC1 to experimental binding energies (cf. Section 3), obviously constant gaps cannot be used in a constrained calculation. Constant gaps that are adjusted to empirical values correspond only to the ground state and, therefore, cannot be used to calculate configurations that generally represent excited states. This is the reason for employing a zero-range pairing force in this example of angular momentum projection and configuration mixing calculation.

The GCM basis is constructed from the self-consistent solution of constrained single-nucleon Dirac equations on a regular mesh in the generating coordinate—the mass quadrupole moment. The corresponding axial deformation parameter spans the interval from $\beta = -0.68$ to $\beta = 1$, with a spacing $\Delta\beta = 0.04$. The GCM basis thus consists of 43 intrinsic states. The large and small components of the Dirac spinors are expanded in a basis of axially symmetric oscillator eigenfunctions for $N = 14$ major shells.

The resulting binding energy curve of ^{154}Sm is shown in Fig. 6, as a function of the axial deformation β. The RMF + BCS mean-field calculation yields a prolate ground-state minimum at $\beta = 0.32$, more than 4.5 MeV deeper than the wide local minimum on the oblate side. One might notice that for prolate shapes the potential is rather stiff with respect to β around the minimum, and this means that the structures built on the ground state will be localized in this minimum, that is, there will be very little mixing with oblate structures for states with relatively low angular momenta. Fig. 6 also displays the corresponding angular-momentum projected ($J^\pi = 0^+, 2^+, 4^+$, and 6^+) energy curves. At this stage we do not consider configuration mixing yet, and the projected energy of the $|\phi(q)\rangle$ state reads

$$E^J(q) = \frac{\mathcal{H}^J(q, q)}{\mathcal{N}^J(q, q)}, \tag{60}$$

where the projected norm overlap kernels

$$\mathcal{N}^J(q, q) = \langle \phi(q) | P^J_{00} | \phi(q) \rangle \tag{61}$$

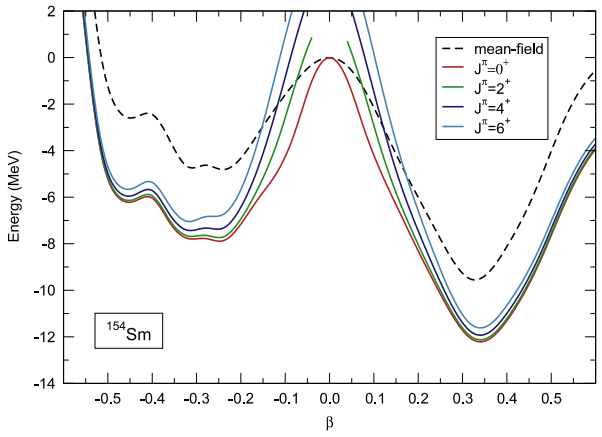

Fig. 6. The RMF + BCS binding energy curve of ^{154}Sm (dashed), and the corresponding angular-momentum projected ($J^\pi = 0^+, 2^+, 4^+$, and 6^+) energy curves, as functions of the axial deformation β.

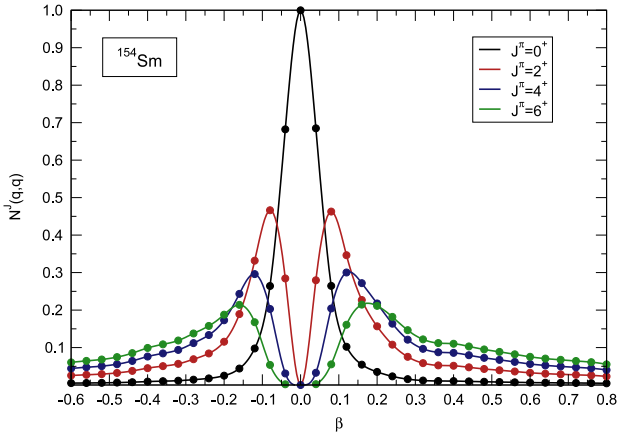

Fig. 7. Projected norm overlap kernels $\mathcal{N}^J(q, q)$ as a functions of the axial quadrupole deformation β.

are plotted in Fig. 7. The spherical configuration is a pure 0^+ state ($\mathcal{N}^{J=0}(0, 0) = 1$), and the maxima of the projected norm overlap kernels for higher angular momenta are correspondingly shifted to larger deformations.

Coming back to the projected energy curves in Fig. 6, we notice that, since the spherical configuration is already a pure 0^+ state, there is no energy gain for $J^\pi = 0^+$ at $\beta = 0$. The rotational energy correction at the prolate minimum $\beta = 0.32$ is more than 2.5 MeV, and even larger in the region of the oblate minimum. The spherical point $\beta = 0$ is not included in the plots of $E^J(q)$ for $J \geq 2$. Namely, for $J \neq 0$ the quantities $\mathcal{H}^J(0, 0)$ and $\mathcal{N}^J(0, 0)$ are so small, that their ratio in Eq. (60) cannot be determined accurately. For higher values of the angular momentum several additional configurations close to the spherical point are also characterized by very small values of the projected norm overlap kernel. These configurations can safely be omitted from the projected energy curves, because on the one hand the angular momentum projection becomes inaccurate at these points, and on the other hand the corresponding angular momentum projected states would not play any role in configuration mixing calculations.

The next step in the solution of the Hill–Wheeler equation (54) is the diagonalization of the norm overlap kernel $\mathcal{N}^J(q_i, q_j)$

$$\sum_j \mathcal{N}^J(q_i, q_j)u_k(q_j) = n_k u_k(q_i). \tag{62}$$

Since the basis functions $|\phi(q_i)\rangle$ are not linearly independent, many eigenvalues n_k will be very close to zero. The corresponding eigenfunctions $u_k(q_i)$ are rapidly oscillating and carry very little physical information. However, due to numerical uncertainties, their contribution to $\tilde{\mathcal{H}}^J(q_i, q_j)$ can be large, and these states should be removed from the basis. From the remaining states one builds the collective Hamiltonian

$$\mathcal{H}^{Jc}_{kl} = \frac{1}{\sqrt{n_k}}\frac{1}{\sqrt{n_l}}\sum_{i,j} u_k(q_i)\tilde{\mathcal{H}}^J(q_i, q_j)u_l(q_j), \tag{63}$$

which is subsequently diagonalized

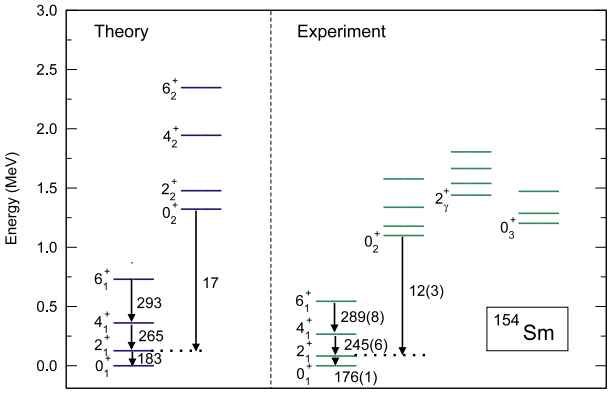

Fig. 8. Angular-momentum projected GCM results for the excitation energies and B(E2) values (in Weisskopf units) of the lowest two bands in ^{154}Sm, in comparison with available data.

$$\sum_{k,l} \mathcal{H}^{Jc}_{kl} g^{J\alpha}_{l} = E^{J}_{\alpha} g^{J\alpha}_{k}. \tag{64}$$

The solution determines both the ground state energy, and the energies of excited states, for each value of the angular momentum J. The collective wave functions $g^J_\alpha(q)$, and the weight functions $f^J_\alpha(q)$, are calculated from the norm overlap eigenfunctions

$$g^J_\alpha(q_i) = \sum_l g^{J\alpha}_l u_l(q_i), \tag{65}$$

and

$$f^J_\alpha(q_i) = \sum_l \frac{g^{J\alpha}_l}{\sqrt{n_l}} u_l(q_i). \tag{66}$$

The GCM excitation energies and the corresponding B(E2) values for the two lowest bands in ^{154}Sm: the ground-state band and the β-band, are displayed in Fig. 8. The results of the angular-momentum projected (AMP) configuration mixing calculation are compared with available data. Since the present calculation is restricted to axial symmetry, it cannot describe structures based on the γ degree of freedom. Considering that, for a given EDF and the effective pairing interaction, the AMP+GCM calculation is parameter-free, the agreement with data is remarkable. One might notice the excellent agreement of the transition probabilities, calculated with the bare proton charge, with the experimental values for transitions within the ground-state band, and the transition from the band-head of the β-band to the ground-state band. The calculated excitation energy of the β band-head is above the experimental 0^+_2, indicating that the potential is probably too stiff with respect to β, and the corresponding moment of inertia appears to be considerably lower than the effective empirical value. The difference between the calculated and empirical moments of inertia is much less pronounced in the ground-state band.

In Fig. 9 we plot the amplitudes of the collective wave functions $|g^J_\alpha(\beta)|^2$ Eq. (65) for the two lowest GCM states of each angular momentum $J^\pi = 0^+, 2^+, 4^+$, and 6^+. The amplitudes in the left panel correspond to the states of the ground-state band, whereas the collective functions of the β-band are plotted in the right panel. For both bands the collective functions are localized in the prolate well, and only for the state 0^+_2 the wave function displays a small amount of oblate admixture.

The treatment of collective correlations in REDF-based structure models has been extended in Ref. [16] to axially symmetric GCM configuration mixing of angular-momentum and particle-number projected states, and very recently a model has been developed that includes triaxial angular-momentum projection [18,19]. The latter does not involve particle number projection. It has to be emphasized that, while GCM configuration mixing of axially symmetric states has been implemented by several groups and routinely used in nuclear structure studies, the application of this method to triaxial shapes presents a much more involved and technically difficult problem. Only the most recent advances in parallel computing and modeling have enabled the implementation of models [84,78], based on triaxial symmetry-breaking intrinsic states, that are projected on particle number and angular momentum, and finally mixed by the generator coordinate method. This implementation is equivalent to a seven-dimensional GCM calculation, mixing all five degrees of freedom of the quadrupole operator and the gauge angles for protons and neutrons. The numerical realization, however, is very complex, and applications to medium-heavy and heavy nuclei are still computationally too demanding and time-consuming. This is true even for a model that does not include particle number projection [19]. In addition, the use of general EDFs with an arbitrary dependence on nucleon densities in GCM-type calculations, often leads to discontinuities or even divergences of the energy kernels as a function of deformation [86,87]. Only for a specific type of density dependence a regularization method can be implemented [88,89], that corrects the energy kernels and removes the discontinuities and divergences. In the next section we therefore review an approximation to the full GCM approach, based on the microscopic REDF framework, that includes rotational symmetry restoration and takes into account triaxial quadrupole fluctuations in arbitrary heavy nuclei.

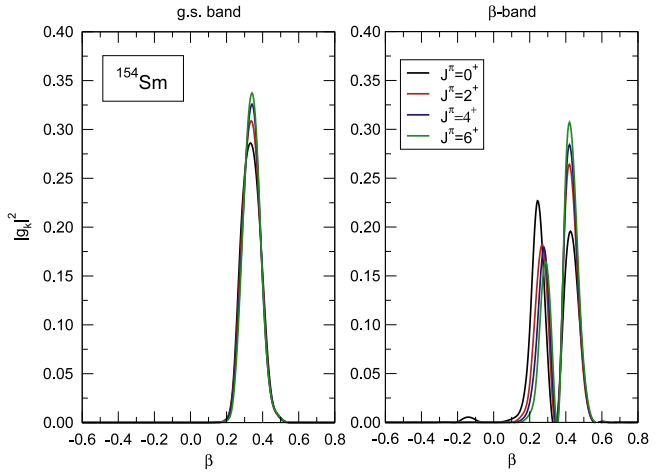

Fig. 9. Amplitudes of the angular-momentum projected GCM collective wave functions $|g^J_\alpha(\beta)|^2$ ($J^\pi = 0^+, 2^+, 4^+$, and 6^+) for the ground-state band (left) and the β-band (right) in ^{154}Sm.

6. Collective Hamiltonian in five dimensions based on relativistic EDFs

In an alternative approach to five-dimensional quadrupole dynamics that restores rotational symmetry and allows for fluctuations around the triaxial mean-field minima, a collective Bohr Hamiltonian can be formulated, with deformation-dependent parameters determined by microscopic self-consistent mean-field calculations. There are two principal approaches to derive the collective Hamiltonian starting from a microscopic framework based on an effective inter-nucleon interaction or energy density functional: (i) the adiabatic approximation to the time-dependent HFB theory (ATDHFB) [90], and (ii) the generator coordinate method (GCM) with the Gaussian overlap approximation (GOA) [91–93]. With the assumption that the GCM overlap kernels can be approximated by Gaussian functions [62], the local expansion of the kernels up to second order in the non-locality transforms the GCM Hill–Wheeler equation into a second-order differential equation—the Schrödinger equation for the collective Hamiltonian. The kinetic part of this Hamiltonian contains an inertia tensor [94], and the potential energy is determined by the diagonal elements of the Hamiltonian kernel, and also includes zero-point energy (ZPE) corrections [95].

The dynamics of the collective Bohr Hamiltonian is determined by the vibrational inertial functions and the moments of inertia [96]. For these quantities either the GCM-GOA (Yoccoz masses [97]) or the ATDHFB expressions (Thouless–Valatin masses [98]) can be used. The Thouless–Valatin masses have the advantage that they also include the time-odd components of the mean-field potential and, in this sense, the full dynamics of a nuclear system. In the GCM approach these components can only be included if, in addition to the coordinates q_i, the corresponding canonically conjugate momenta p_i are also taken into account, but this is obviously a very complicated task. In many applications a further simplification is thus introduced in terms of cranking formulas [99,95], that represent the perturbative limit for the Thouless–Valatin masses, and the corresponding expressions for ZPE corrections. This approximation was applied in recent studies using models based both on the Gogny interaction [100,101], and Skyrme energy density functionals [102,93]. The approximate inclusion of Thouless–Valatin corrections to the mass parameters and moments of inertia of the Skyrme-based Bohr Hamiltonian was discussed in Ref. [102]. In a recent systematic study [103] of low-energy nuclear structure at normal deformation, based on the Hartree–Fock–Bogoliubov theory extended by the generator coordinate method and mapped onto a five-dimensional collective quadrupole Hamiltonian, the Thouless–Valatin moments of inertia were used, whereas the cranking approximation was used for the quadrupole mass parameters. Using the Gogny D1S interaction, even–even nuclei with proton numbers $Z = 10$ to $Z = 110$ and neutron numbers $N \leq 200$ were calculated.

Here we review a recent implementation for the solution of the eigenvalue problem of a five-dimensional collective Hamiltonian for quadrupole vibrational and rotational degrees of freedom, with parameters determined by constrained self-consistent relativistic Hartree–Bogoliubov calculations for triaxial shapes [104,17,105–107,67].

6.1. Collective Hamiltonian

The general Bohr collective model for the description of quadrupole collective states, including a detailed discussion of the model's kinematics, has recently been reviewed in Ref. [93]. Nuclear excitations determined by quadrupole vibrational and rotational degrees of freedom can be treated simultaneously by considering five quadrupole collective coordinates $\alpha_\mu,\ \mu = -2, -1, \ldots, 2$ that describe the surface of a deformed nucleus: $R = R_0\left[1 + \sum_\mu \alpha_\mu Y^*_{2\mu}\right]$. To separate rotational and vibrational motion, these coordinates are usually parameterized in terms of two deformation parameters β and γ, and three Euler angles $(\phi, \theta, \psi) \equiv \Omega$ that define the orientation of the intrinsic principal axes in the laboratory frame

$$\alpha_\mu = D^2_{\mu 0}(\Omega)\beta\cos\gamma + \frac{1}{\sqrt{2}}\left[D^2_{\mu 2}(\Omega) + D^2_{\mu -2}(\Omega)\right]\beta\sin\gamma, \tag{67}$$

where $D^\lambda_{\mu\nu}$ is the Wigner function. The three terms of the classical collective Hamiltonian, expressed in terms of the intrinsic variables β, γ and Euler angles

$$H_{\rm coll} = \mathcal{T}_{\rm vib}(\beta,\gamma) + \mathcal{T}_{\rm rot}(\beta,\gamma,\Omega) + \mathcal{V}_{\rm coll}(\beta,\gamma), \tag{68}$$

denote the contributions from the vibrational kinetic energy:

$$\mathcal{T}_{\rm vib} = \frac{1}{2}B_{\beta\beta}\dot\beta^2 + \beta B_{\beta\gamma}\dot\beta\dot\gamma + \frac{1}{2}\beta^2 B_{\gamma\gamma}\dot\gamma^2, \tag{69}$$

the rotational kinetic energy:

$$\mathcal{T}_{\rm rot} = \frac{1}{2}\sum_{k=1}^{3}\mathcal{I}_k\omega_k^2, \tag{70}$$

and the collective potential energy $\mathcal{V}_{\rm coll}(\beta,\gamma)$. The mass parameters $B_{\beta\beta}$, $B_{\beta\gamma}$, $B_{\gamma\gamma}$, and the moments of inertia $\mathcal{I}_k$ depend on the quadrupole deformation variables β and γ.

After quantization the classical kinetic energy of the Hamiltonian equation (68):

$$T = \frac{1}{2}\sum_{ij}B_{ij}(q)\dot q_i\dot q_j, \tag{71}$$

reads:

$$\hat H_{\rm kin} = -\frac{\hbar^2}{2}\frac{1}{\sqrt{\det B}}\sum_{ij}\frac{\partial}{\partial q_i}\sqrt{\det B}(B^{-1})_{ij}\frac{\partial}{\partial q_j}. \tag{72}$$

The kinetic energy tensor takes the block diagonal form:

$$B = \begin{pmatrix} B_{\rm vib} & 0 \\ 0 & B_{\rm rot}\end{pmatrix}, \tag{73}$$

with the vibrational part of the tensor

$$B_{\rm vib} = \begin{pmatrix} B_{\beta\beta} & \beta B_{\beta\gamma} \\ \beta B_{\beta\gamma} & \beta^2 B_{\gamma\gamma}\end{pmatrix}. \tag{74}$$

In general, the rotational part is a complicated function of the Euler angles but, using the quasi-coordinates related to the components of the angular momentum in the body-fixed frame, it takes a simple diagonal form

$$(B_{\rm rot})_{ik} = \delta_{ik}\mathcal{I}_k, \quad k = 1,2,3, \tag{75}$$

with the moments of inertia expressed as

$$\mathcal{I}_k = 4B_k\beta^2\sin^2(\gamma - 2k\pi/3). \tag{76}$$

This particular functional form is motivated by the fact that all three moments of inertia vanish for the spherical configuration ($\beta = 0$) and, additionally, $\mathcal{I}_z$ and $\mathcal{I}_y$ vanish for axially symmetric prolate ($\gamma = 0°$) and oblate ($\gamma = 60°$) configurations, respectively. The resulting determinant reads

$$\det B = \det B_{\rm vib}\cdot\det B_{\rm rot} = 4wr\beta^8\sin^2 3\gamma, \tag{77}$$

where $w = B_{\beta\beta}B_{\gamma\gamma} - B^2_{\beta\gamma}$ and $r = B_1B_2B_3$. The quantized collective Hamiltonian can hence be written in the form:

$$\hat H = \hat T_{\rm vib} + \hat T_{\rm rot} + V_{\rm coll}, \tag{78}$$

with

$$\begin{aligned}\hat T_{\rm vib} = -\frac{\hbar^2}{2\sqrt{wr}}\Bigg\{&\frac{1}{\beta^4}\left[\frac{\partial}{\partial\beta}\sqrt{\frac{r}{w}}\beta^4 B_{\gamma\gamma}\frac{\partial}{\partial\beta} - \frac{\partial}{\partial\beta}\sqrt{\frac{r}{w}}\beta^3 B_{\beta\gamma}\frac{\partial}{\partial\gamma}\right]\\ &+\frac{1}{\beta\sin 3\gamma}\left[-\frac{\partial}{\partial\gamma}\sqrt{\frac{r}{w}}\sin 3\gamma B_{\beta\gamma}\frac{\partial}{\partial\beta} + \frac{1}{\beta}\frac{\partial}{\partial\gamma}\sqrt{\frac{r}{w}}\sin 3\gamma B_{\beta\beta}\frac{\partial}{\partial\gamma}\right]\Bigg\},\end{aligned} \tag{79}$$

and

$$\hat T_{\rm rot} = \frac{1}{2}\sum_{k=1}^{3}\frac{\hat J_k^2}{\mathcal{I}_k}, \tag{80}$$

where $\hat{J}_k$ denotes the components of the angular momentum in the body-fixed frame of a nucleus. $V_{\rm coll}$ is the collective potential. The Hamiltonian describes quadrupole vibrations, rotations, and the coupling of these collective modes. The determinant Eq. (77) determines the volume element in the collective space:

$$\int \mathrm{d}\tau_{\rm coll} = \int \mathrm{d}\Omega \mathrm{d}\tau_0 \sqrt{wr} = \int_0^\infty \mathrm{d}\beta \beta^4 \int_0^{2\pi} \mathrm{d}\gamma |\sin 3\gamma| \int \mathrm{d}\Omega \sqrt{wr}, \tag{81}$$

and the quantized Hamiltonian equation (78) is hermitian with respect to the collective measure Eq. (81).

The eigenvalue problem of the general collective Hamiltonian equation (78) can be solved by a direct numerical solution of a system of partial differential equations using finite-difference methods, or by employing an expansion of eigenfunctions in terms of a truncated basis in the collective Hilbert space. The basis functions depend on the deformation variables β and γ, and the Euler angles ϕ, θ and ψ. In the latter case the eigenvalue problem reduces to a simple matrix diagonalization, and the main task is the construction of an appropriate basis for each value of the angular momentum quantum number. In the implementation developed in Ref. [17] we employed the basis expansion approach.

The diagonalization of the Hamiltonian yields the excitation energies and collective wave functions:

$$\Psi_\alpha^{IM}(\beta, \gamma, \Omega) = \sum_{K \in \Delta J} \psi_{\alpha K}^J(\beta, \gamma) \Phi_{MK}^J(\Omega). \tag{82}$$

The angular part corresponds to a linear combination of Wigner functions

$$\Phi_{MK}^J(\Omega) = \sqrt{\frac{2J+1}{16\pi^2(1+\delta_{K0})}} \left[D_{MK}^{J*}(\Omega) + (-1)^J D_{M-K}^{J*}(\Omega) \right], \tag{83}$$

and the summation in Eq. (82) is over the allowed set of the K values:

$$\Delta J = \begin{cases} 0, 2, \ldots, J & \text{for } J \bmod 2 = 0 \\ 2, 4, \ldots, J-1 & \text{for } J \bmod 2 = 1. \end{cases} \tag{84}$$

Using the collective wave functions Eq. (82), various observables can be calculated and compared with experimental results. For instance, the quadrupole E2 reduced transition probability:

$$B(\mathrm{E2}; \alpha J \to \alpha' J') = \frac{1}{2J+1} |\langle \alpha' J' | | \hat{\mathcal{M}}(\mathrm{E2}) | | \alpha J \rangle|^2, \tag{85}$$

where $\hat{\mathcal{M}}(\mathrm{E2})$ is the electric quadrupole operator. For the $\hat{\mathcal{M}}(\mathrm{E2})$ matrix elements the current implementation of the model uses a local expression in the collective deformation variables [108]. This approximation is justified in the case of large overlaps between different vibrational amplitudes [100], but may be less suited for transitions between states with a rather small overlap, e.g. for transitions between super-deformed bands and bands at normal deformation.

The shape of a nucleus can be characterized in a qualitative way by the average values of the invariants β^2, $\beta^3 \cos 3\gamma$, as well as their combinations. For example, the average value of the invariant β^2 in the state $|\alpha J\rangle$:

$$\langle \beta^2 \rangle_{J\alpha} = \langle \Psi_\alpha^J | \beta^2 | \Psi_\alpha^J \rangle = \sum_{K \in \Delta J} \int \beta^2 |\psi_{\alpha,K}^J(\beta, \gamma)|^2 \mathrm{d}\tau_0, \tag{86}$$

and the average values of the deformation parameters β and γ in the state $|\alpha J\rangle$ are calculated from:

$$\langle \beta \rangle_{J\alpha} = \sqrt{\langle \beta^2 \rangle_{J\alpha}}, \tag{87}$$

$$\langle \gamma \rangle_{J\alpha} = \frac{1}{3} \arccos \frac{\langle \beta^3 \cos 3\gamma \rangle_{J\alpha}}{\sqrt{\langle \beta^2 \rangle_{J\alpha} \langle \beta^4 \rangle_{J\alpha}}}. \tag{88}$$

The mixing of different intrinsic configurations in the state $|\alpha I\rangle$ can be determined from the distribution of the projection K of the angular momentum I on the z axis in the body-fixed frame:

$$N_K = 6 \int_0^{\pi/3} \int_0^\infty |\psi_{\alpha,K}^J(\beta, \gamma)|^2 \beta^4 |\sin 3\gamma| \mathrm{d}\beta \mathrm{d}\gamma, \tag{89}$$

where the components $\psi_{\alpha,K}^J(\beta, \gamma)$ are defined in Eq. (82). For large deformations the K quantum number is to a good approximation conserved. Consequently, only one of the integrals Eq. (89) will give a value close to 1. A broader distribution of N_K values in the state $|\alpha J\rangle$ provides a measure of mixing of intrinsic configurations.

6.2. Microscopic parameters of the collective Hamiltonian

The entire dynamics of the collective Hamiltonian is governed by the seven functions of the intrinsic deformations β and γ: the collective potential, the three mass parameters: $B_{\beta\beta}, B_{\beta\gamma}, B_{\gamma\gamma}$, and the three moments of inertia $\mathcal{I}_k$. These functions

are determined by the choice of a particular microscopic nuclear energy density functional or effective interaction. The entire map of the energy surface as a function of the quadrupole deformation is obtained by imposing constraints on the axial and triaxial mass quadrupole moments, as described in Section 4. The quasiparticle wave functions and energies, generated from constrained self-consistent solutions of the RHB model, provide the microscopic input for the parameters of the collective Hamiltonian.

In the simplest approximation the moments of inertia are calculated from the Inglis–Belyaev formula:

$$\mathcal{I}_k = \sum_{i,j} \frac{|\langle ij|\hat{J}_k|\Phi\rangle|^2}{E_i + E_j} \quad k = 1, 2, 3, \tag{90}$$

where k denotes the axis of rotation, the summation runs over proton and neutron quasiparticle states $|ij\rangle = \beta_i^\dagger \beta_j^\dagger |\Phi\rangle$, and $|\Phi\rangle$ represents the quasiparticle vacuum. The mass parameters associated with the two quadrupole collective coordinates $q_0 = \langle\hat{Q}_{20}\rangle$ and $q_2 = \langle\hat{Q}_{22}\rangle$ are calculated in the cranking approximation:

$$B_{\mu\nu}(q_0, q_2) = \frac{\hbar^2}{2}\left[\mathcal{M}_{(1)}^{-1}\mathcal{M}_{(3)}\mathcal{M}_{(1)}^{-1}\right]_{\mu\nu}, \tag{91}$$

where

$$\mathcal{M}_{(n),\mu\nu}(q_0, q_2) = \sum_{i,j} \frac{\left|\langle\Phi|\hat{Q}_{2\mu}|ij\rangle\langle ij|\hat{Q}_{2\nu}|\Phi\rangle\right|}{(E_i + E_j)^n}. \tag{92}$$

The collective energy surface includes the energy of the zero-point motion, and this quantity has to be subtracted. The collective zero-point energy (ZPE) corresponds to a superposition of zero-point motion of individual nucleons in the single-nucleon potential. In the general case, the ZPE corrections on the potential energy surfaces depend on the deformation. The ZPE includes terms originating from the vibrational and rotational kinetic energy, and a contribution of potential energy

$$\Delta V(q_0, q_2) = \Delta V_{\text{vib}}(q_0, q_2) + \Delta V_{\text{rot}}(q_0, q_2) + \Delta V_{\text{pot}}(q_0, q_2). \tag{93}$$

The latter is much smaller than the contribution of the kinetic energy, and is usually neglected [100]. Simple prescriptions for the calculation of vibrational and rotational ZPE have been derived in Ref. [95]. Both corrections are calculated in the cranking approximation, i.e. on the same level of approximation as the mass parameters and the moments of inertia. The vibrational ZPE is given by the expression:

$$\Delta V_{\text{vib}}(q_0, q_2) = \frac{1}{4}\text{Tr}\left[\mathcal{M}_{(3)}^{-1}\mathcal{M}_{(2)}\right]. \tag{94}$$

The rotational ZPE is a sum of three terms:

$$\Delta V_{\text{rot}}(q_0, q_2) = \Delta V_{-2-2}(q_0, q_2) + \Delta V_{-1-1}(q_0, q_2) + \Delta V_{11}(q_0, q_2), \tag{95}$$

with

$$\Delta V_{\mu\nu}(q_0, q_2) = \frac{1}{4}\frac{\mathcal{M}_{(2),\mu\nu}(q_0, q_2)}{\mathcal{M}_{(3),\mu\nu}(q_0, q_2)}. \tag{96}$$

The individual terms are calculated from Eqs. (96) and (92), with the intrinsic components of the quadrupole operator defined by:

$$\hat{Q}_{21} = -2\text{i}yz, \qquad \hat{Q}_{2-1} = -2xz, \qquad \hat{Q}_{2-2} = 2\text{i}xy. \tag{97}$$

The potential V_{coll} in the collective Hamiltonian equation (78) is obtained by subtracting the ZPE corrections from the total mean-field energy:

$$V_{\text{coll}}(q_0, q_2) = E_{\text{tot}}(q_0, q_2) - \Delta V_{\text{vib}}(q_0, q_2) - \Delta V_{\text{rot}}(q_0, q_2). \tag{98}$$

As an example in Fig. 10 we display the spectrum of collective states of ^{240}Pu. Starting from constrained self-consistent solutions of the RHB equations, i.e. using single-quasiparticle energies and wave functions that correspond to each point on the energy surface shown in Fig. 4, the parameters of the collective Hamiltonian are calculated as functions of the deformations β and γ. The diagonalization of the Hamiltonian yields the excitation spectrum shown in Fig. 10, shown in comparison to data for the three lowest positive-parity bands at normal deformation, and the lowest $\pi = +$ super-deformed band of ^{240}Pu. In addition to the yrast ground-state band, in deformed and transitional nuclei excited states are also assigned to (quasi) β and γ bands. This is done according to the distribution of the projection K of the angular momentum I on the z axis of the body-fixed frame Eq. (89). Excited states with predominant $K = 2$ components in the wave function are assigned to the γ-band, whereas the β-band comprises the states above the yrast characterized by dominant $K = 0$ components. $K = 0$ states are assigned to the super-deformed band based on the calculated average value of the deformation parameter β Eq. (87).

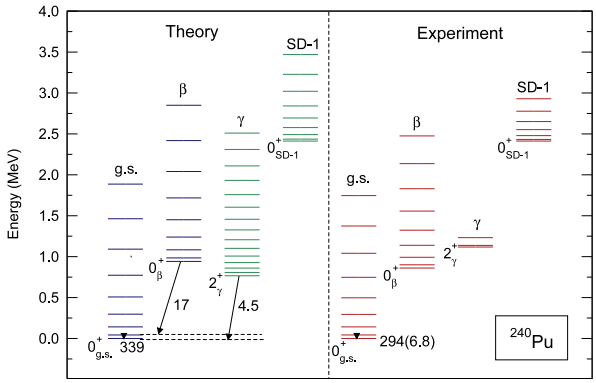

Fig. 10. The low-energy spectrum of ^{240}Pu calculated with the DD-PC1 relativistic density functional (left), compared with data (right) for the three lowest positive-parity bands at normal deformation, and the lowest $\pi = +$ superdeformed band.

The Inglis–Belyaev (IB) moments of inertia Eq. (90) of the collective Hamiltonian have been multiplied by a common factor so that the calculated energy of the 2_1^+ state coincides with the experimental value. This scale parameter reflects the well known fact that the IB expression predicts effective moments of inertia that are smaller than empirical values. In the calculation of the spectrum of ^{240}Pu we have thus followed the prescription of Ref. [100] where, by comparing the more realistic, but also computationally more involved, Thouless–Valatin (TV) moments of inertia with the IB values as functions of the axial deformation for superdeformed bands in the $A \approx 190$ mass region, it was shown that the TV correction to the perturbative IB expression is almost independent of deformation, and does not include significant new structures in the moments of inertia. It was thus suggested that the moments of inertia to be used in the collective Hamiltonian can be simply related to the IB values through the minimal prescription: $\mathcal{I}_k(q) = \mathcal{I}_k^{\mathrm{IB}}(q)(1+\alpha)$, where q denotes the generic deformation parameter, and α is a constant that can be determined in comparison to data. In the present case $\alpha = 0.32$ for ^{240}Pu.

When the IB effective moment of inertia is renormalized to the empirical value, the excitation spectrum of the collective Hamiltonian determined by the functional DD-PC1 is in very good agreement with the available data for the ground-state band, β and γ bands, and even the lowest super-deformed band SD-1. Compared to the corresponding experimental sequence, the position of the γ band is predicted at a somewhat lower excitation energy, and this might indicate that the theoretical PES is probably too soft in γ. The β-band is calculated at a slightly higher energy compared to the experiment, and the predicted position of SD-1 is within the experimental error bounds. Very little data are available on electromagnetic transition rates in ^{240}Pu. In fact, except for the lifetime of the 2_1^+ state, only the lifetimes of K-isomers have been measured but these include configurations not contained in our collective model space. Therefore, in Fig. 10 we only display the calculated B(E2) values, in Weisskopf units (W.u.), for the transition $2_1^+ \rightarrow 0_1^+$ and from the band-heads of the β and γ bands to the ground-state band. It should be emphasized that besides the renormalization of the moment of inertia, the calculation is completely parameter-free, i.e. by using structure models based on self-consistent mean-field single-particle solutions, physical observables, such as transition probabilities and spectroscopic quadrupole moments, are calculated in the full configuration space and there is no need for effective charges. Using the bare value of the proton charge in the electric quadrupole operator $\hat{\mathcal{M}}$(E2), the transition probabilities between eigenstates of the collective Hamiltonian can be directly compared to data.

6.3. Illustrative calculation: evolution of triaxial shapes in Pt isotopes

Most deformed nuclei display axially-symmetric prolate ground-state shapes, but some regions of the nuclide chart are characterized by the occurrence of oblate deformed and triaxial shapes. One of the examples is the $A \approx 190$ mass region, where both prolate to oblate shape transitions, as well as triaxial ground-state shapes have been predicted. An extensive analysis of this region has recently been performed using non-relativistic Skyrme and Gogny interactions [109,110]. The self-consistent Hartree–Fock–Bogoliubov model has been used to study the evolution of the ground-state shapes of Yb, Hf, W, Os and Pt isotopes. In particular, it has been shown that the isotopic chains with larger Z-numbers in this mass region display a tendency toward triaxial shapes. Here we present the 3D RHB binding energy maps for the sequence of even-A Pt isotopes with neutron numbers in the interval from $N = 108$ to $N = 126$, calculated with the DD-PC1 energy density functional plus the pairing interaction Eq. (34).

In Table 1 we list the calculated values of the β and γ deformation parameters for the absolute minima of the potential energy surfaces (PES). One can follow the transition from the prolate deformed ^{186}Pt, through the region of triaxially deformed $^{188-198}$Pt isotopes, to the slightly oblate ^{200}Pt, and finally the spherical $^{202-204}$Pt isotopes. The ground-state β-deformation steadily decreases as the number of neutrons increases and approaches the closed-shell at $N = 126$. In order to analyze the nature of shape transition in the Pt isotopic chain, in Fig. 11 we display the self-consistent RHB quadrupole binding energy maps of the even-$A^{190-200}$Pt isotopes in the $\beta - \gamma$ plane ($0^\circ \leq \gamma \leq 60^\circ$). All energies are normalized with

Table 1
Calculated values of the β and γ deformation parameters for the absolute minima of the potential-energy surfaces (PES) of even-A Pt isotopes with $186 \leq A \leq 204$.

A	186	188	190	192	194	196	198	200	202	204
β	0.30	0.28	0.19	0.18	0.15	0.13	0.12	0.08	0	0
γ	0°	9°	34°	34°	34°	31°	33°	60°	0°	0°

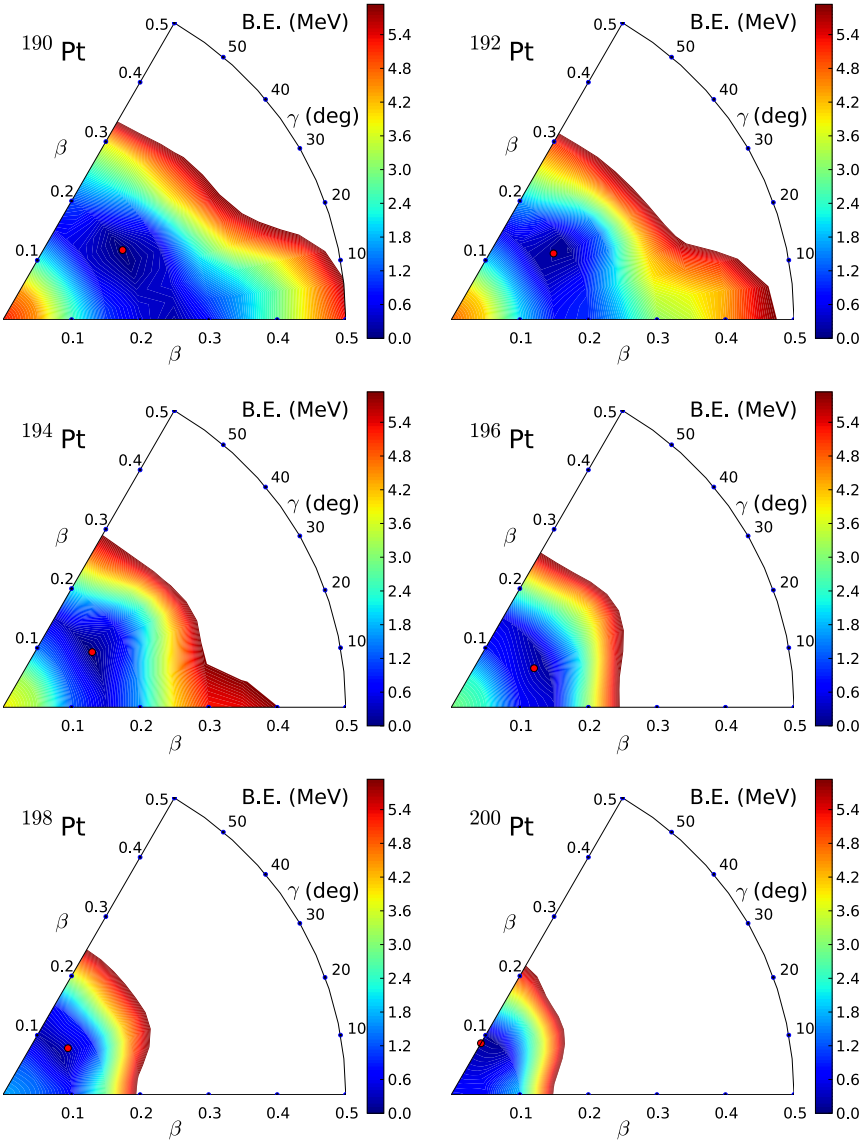

Fig. 11. Self-consistent RHB triaxial quadrupole binding-energy maps of the even–even isotopes $^{190-200}$Pt in the $\beta - \gamma$ plane ($0 \leq \gamma \leq 60°$). All energies are normalized with respect to the binding energy of the absolute minimum (red dot). (For interpretation of the references to colour in this figure legend, the reader is referred to the web version of this article.)

respect to the binding energy of the absolute minimum, and the color code refers to the energy of each point on the surface relative to the minimum. The PES of $^{190-198}$Pt are γ-soft, with shallow minima at $\gamma \approx 30°$. The nucleus ^{200}Pt displays a slightly oblate minimum, signaling the shell-closure at $N = 126$.

As an illustrative example for the microscopic origin of the triaxial ground-state deformations, we consider the nucleus ^{192}Pt. The formation of deformed minima can be related to the occurrence of gaps or regions of low single-particle level density around the Fermi surface. In Figs. 12 and 13 we plot the proton and neutron single-particle energy levels in the canonical basis for ^{192}Pt. Solid curves correspond to levels with positive parity, and short-dashed curves denote levels with negative parity. The long-dashed (yellow) curve corresponds to the Fermi level. The leftmost and the rightmost panels

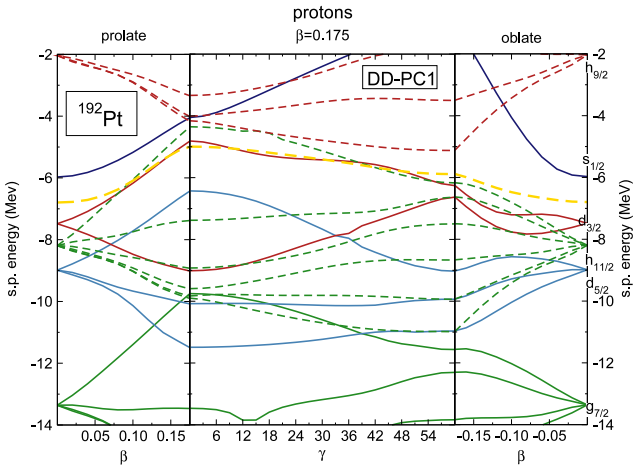

Fig. 12. Proton canonical single-particle energy levels of ^{192}Pt. Solid curves denote levels with positive parity and short-dashed curves levels with negative parity. The long-dashed (yellow) curve corresponds to the Fermi level. The leftmost and the rightmost panels display prolate and oblate axially symmetric single-particle levels, respectively. The middle panel shows the single-particle levels as functions of γ for the fixed value of the axial deformation $|\beta| = 0.18$. (For interpretation of the references to colour in this figure legend, the reader is referred to the web version of this article.)

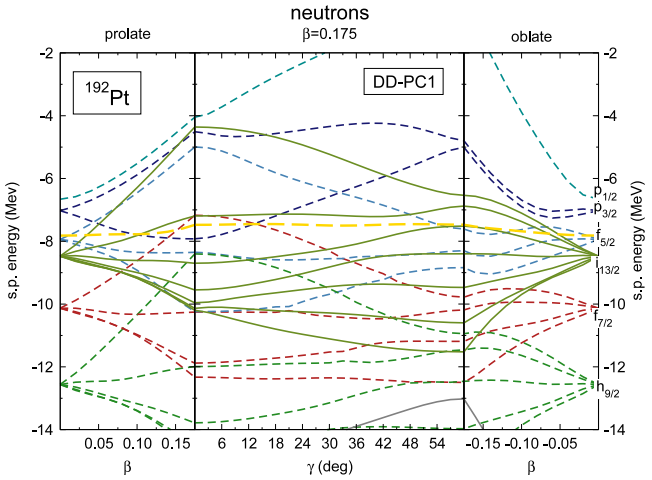

Fig. 13. Same as described in the caption to Fig. 12 but for neutron single-particle levels.

display prolate and oblate axially-symmetric single-particle levels, respectively, whereas the middle panel shows the single-particle levels as functions of γ for the fixed value of the axial deformation $|\beta| = 0.18$. This type of plot has been introduced in Ref. [111], and it enables the identification of K quantum numbers of triaxial single-particle levels in the limits of axial symmetry at $\gamma = 0^\circ$ and $\gamma = 60^\circ$ [109,110,112].

In Fig. 12 we notice the occurrence of a gap between the proton single-particle levels in the vicinity of the Fermi surface around $\gamma = 30^\circ$. The energy gap predominantly results from the down-sloping of one particular single-particle orbital, originating from the spherical $d_{5/2}$ shell, as the deformation parameter γ increases from $\gamma = 0^\circ$ to $\gamma = 60^\circ$. This result is in agreement with the findings of Ref. [109]. The corresponding neutron single-particle levels, shown in Fig. 13, also display a region of low level density around the Fermi surface at $\gamma \approx 30^\circ$, although the gap is somewhat less pronounced in comparison to the proton gap.

The low-energy spectra of ^{192}Pt and ^{194}Pt, obtained by diagonalization of the collective Hamiltonian based on the DD-PC1 energy density functional plus the pairing interaction Eq. (34), are displayed in Figs. 14 and 15. The calculated ground-state bands and (quasi) γ-bands are compared with the corresponding sequences of experimental states. Both the theoretical excitation energies and B(E2) values are in very good agreement with data. In the case of Pt isotopes it was not necessary to renormalize the effective moments of inertia, i.e. the spectra shown in Figs. 14 and 15 do not include any additional scaling parameter. As already emphasized, transition probabilities are calculated in the full configuration space with bare proton charges. In particular, one might notice the excellent result for the predicted excitation energy of the bandhead of the γ-band in both nuclei, as well as the very good agreement with the experimental B(E2) values for transitions between the γ-band and the yrast band. This result indicates that the DD-PC1 potential has the correct stiffness with respect to the γ

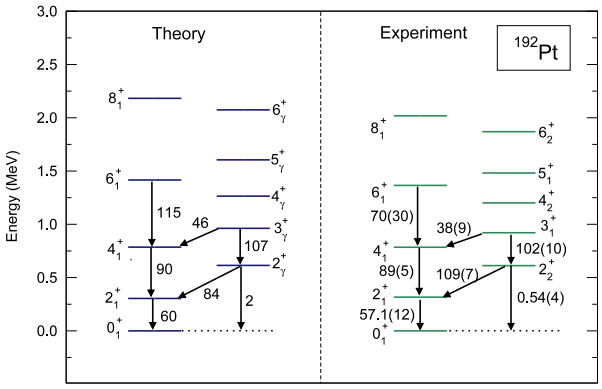

Fig. 14. The low energy spectrum of ^{192}Pt calculated with the DD-PC1 relativistic density functional (left) compared with the data (right) for the excitation energies and intraband and interband B(E2) values (in Weisskopf units).

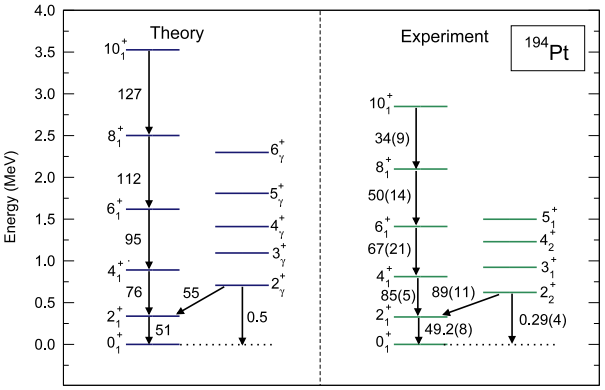

Fig. 15. Same as described in the caption to Fig. 14 but for the isotope ^{194}Pt.

degree of freedom. A similar agreement with data is also obtained in the calculation of low-energy spectra for the other Pt isotopes whose PES are displayed in Fig. 11.

The five-dimensional collective Hamiltonian for quadrupole vibrational and rotational degrees of freedom, with parameters determined by constrained self-consistent relativistic mean-field calculations for triaxial shapes, has also been employed in studies of microscopic signatures of ground-state shape phase transitions in Nd isotopes around $N = 90$ [105,106], and Ba and Xe nuclei in the mass $A \approx 130$ region [107]. A detailed comparison with available data and with predictions of the analytical X(5) [113] and E(5) [114] models, has shown that the microscopic theoretical framework based on relativistic EDFs describes not only general features of shape transitions, but also singular properties of excitation spectra and transition rates at the points of first- and second-order quantum shape phase transitions.

There are possible improvements and extensions of the model that has been reviewed in this section. For instance, because in most cases the Inglis–Belyaev formula yields effective moments of inertia that are lower than empirical values, all the calculated relative excitation energies had to be scaled with respect to the experimental energy of the 2_1^+ states. The moments of inertia can be improved by including the Thouless–Valatin dynamical rearrangement contributions. For the rotational degrees of freedom for which the collective momenta are known, the inertia parameters can be obtained from the solutions of cranked RHB equations. For the deformation coordinates q_0 and q_2 the situation is more complicated, because the corresponding momentum operators $\hat{P}_0$ and $\hat{P}_2$ have to be calculated from the solution of Thouless–Valatin equations [98] at each deformation point. Because cranking breaks time-reversal symmetry, in both cases the inclusion of pairing correlations necessitates calculations in the full relativistic Hartree–Bogoliubov framework, including time-odd components of the nucleon self-energies.

7. Summary and outlook

A wealth of new data from radioactive-beam facilities, the exciting phenomenology of nuclear astrophysics, and recent theoretical developments in related fields, have prompted important advances in theoretical nuclear structure physics during the last decade. The objective of this field is to build a consistent microscopic framework that will, on the one hand, bridge the gap between the underlying theory of strong interactions and the phenomenology of finite nuclei and, on the other, provide a unified description of bulk properties, excitations and reactions across the entire chart of nuclides.

Even though *ab initio* approaches, starting from a microscopic nuclear Hamiltonian that accurately reproduces scattering and few-body data, have been very successful in the description of relatively light nuclei up to oxygen isotopes, and large-scale semi-microscopic shell model calculations are performed for medium-heavy and even some heavy nuclei in the vicinity of closed shells, at present the only comprehensive approach to nuclear structure is provided by the framework of energy density functionals. The advantages of using EDFs in the description of structure phenomena are evident already at the basic level of implementation—the self-consistent mean-field method: an intuitive interpretation of mean-field results in terms of intrinsic shapes and single-particle states, calculations are performed in the full model space of occupied states (no distinction between core and valence nucleons, no need for effective charges), and the universality of EDFs that enables their applications to *all* nuclei throughout the periodic chart. The latter feature is especially important for extrapolations to regions of exotic short-lived nuclei far from stability for which few, if any, data are available. For spectroscopic applications, however, the EDF-based approach must be extended beyond the static mean-field level and models must be developed that include collective correlations related to the restoration of broken symmetries in finite nuclei, and take into account fluctuations of collective variables around mean-field minima.

Relativistic energy density functionals (REDFs) have their origin in the highly successful relativistic mean-field (RMF) phenomenological models introduced by Walecka and Serot [8,9], and later applied and further developed by many groups. More recently, this framework has been reinterpreted by analogy to the relativistic Kohn–Sham density functional theory. It has been realized that the original meson-exchange forces used in RMF models present only one of the possible representations of the effective in-medium inter-nucleon interactions and, moreover, one that does not present any particular advantage at low energies characteristic for nuclear binding and low-lying excitations. Functionals have thus been developed that are expressed in terms of ground-state nucleon four-currents and scalar densities only, with short-distance correlations and long-range dynamics represented either by higher order powers of the currents and densities, or encoded in the medium (nucleon density) dependence of the coupling functions of interaction Lagrangians. The corresponding structure models have been applied to studies of a variety of phenomena in spherical and deformed nuclei, extending over the whole mass table and to systems with extreme isospin values. The illustrative calculations presented in this work have been performed using the relativistic energy density functional DD-PC1 [34] for which, starting from microscopic nucleon self-energies in nuclear matter, the parameters were fine-tuned in a careful fit to experimental binding energies of 64 axially deformed nuclei in the mass regions $A \approx 150$–180 and $A \approx 230$–250. For quantitative calculations in open-shell nuclei it also necessary to consider pairing correlations and, when used in the relativistic Hartree–Bogoliubov (RHB) framework together with a pairing force separable in momentum space, the functional DD-PC1 provides an excellent description of ground-state properties. The corresponding self-consistent QRPA calculations reproduce the excitation energies of giant multipole resonances.

In this work we have also reviewed the latest extensions of the REDF framework that include the treatment of collective correlations. By restoring symmetries broken by the static mean-field and considering fluctuations of collective deformation variables, REDF-based models have been developed that can be employed in detailed spectroscopic studies, including predictions for excitation spectra and electromagnetic transitions. For axially deformed nuclei this approach has been illustrated by GCM configuration mixing calculations of angular-momentum projected relativistic mean-field wave functions. The GCM excitation energies and the corresponding B(E2) values for the two lowest bands in ^{154}Sm have been discussed in comparison with available data. In an approximation to the full GCM treatment of the five-dimensional quadrupole dynamics, a collective Bohr Hamiltonian has been formulated, with deformation-dependent parameters determined by constrained microscopic self-consistent RHB calculations of triaxial energy surfaces in the $\beta - \gamma$ plane. The entire map of the energy surface as function of the quadrupole deformation is obtained by imposing constraints on the mass quadrupole moments. The quasiparticle wave functions and energies, generated from constrained self-consistent solutions of the RHB model, provide the microscopic input for the parameters of the collective Hamiltonian: the collective potential, the three mass parameters: $B_{\beta\beta}$, $B_{\beta\gamma}$, $B_{\gamma\gamma}$, and the three moments of inertia $\mathcal{I}_k$. The implementation of this complex, REDF-based, microscopic collective model has been exemplified in a study of the evolution of triaxial shapes in Pt isotopes. The DD-PC1 based 3D RHB calculation provides a simple microscopic interpretation of the occurrence of triaxial shapes in terms of proton and neutron single-particle levels, and the calculated ground-state bands and (quasi) γ-bands are in very good agreement with the corresponding sequences of experimental states, both for the excitation energies and B(E2) values.

In the remainder of this section we outline some of the most important challenges for the framework of (relativistic) density functionals.

An important issue is the development of a series (ladder) of accurate and controlled approximation for the exchange–correlation terms of the energy density functional, analogous to the "Jacob's Ladder" of Coulomb Density Functional Theory [115]. One possible approach is to develop the exchange–correlation functional from first principles by incorporating known exact constraints, another is empirical and optimizes a parametric ansatz by adjusting it to a set of data. In the context of nuclear density functionals this topic has recently been discussed in the review of Ref. [6], and a possible non-empirical approach to climbing the rungs of the ladder of approximations toward the universal functional has been indicated.

A related topic is the link between the framework of nuclear EDFs and the underlying theory of strong interaction–low-energy QCD, which will include both nuclear matter and finite nuclei. At low energies characteristic for nuclear binding, QCD is realized as a theory of pions coupled to nucleons [116]. The basic concept of a low-energy effective field theory (EFT) is the

separation of scales: the long-range physics (pion exchange) is treated explicitly, whereas short-distance interactions, that cannot be resolved at low energy, are replaced by contact terms. In a non-empirical approach to nuclear NEDFs, the EFT-based derivation of exchange–correlation functionals in principle allows for error estimates, and provides a power counting scheme that separates long- and short-distance dynamics.

Even a non-empirical universal energy density functional will have to be fine-tuned to data on medium-heavy and heavy nuclei. This is because such a functional contains a number of low-energy constants that determine the strength of the leading short-range interactions. These constants cannot be adjusted already from scattering and few-body data to an accuracy that enables a quantitative description of structure phenomena in complex nuclear systems. In principle any complete set of low-energy data, for instance experimental masses, can be used to fine-tune the EDF. However, when only a small number of nuclei is considered, satisfactory *least-squares* fits can be obtained with different, in general linearly dependent combinations of parameters. Moreover, ground states of spherical nuclei that have mostly been used to adjust functionals or effective interactions, include collective correlations that cannot be absorbed in a universal functional. Another important issue concerns functionals that are used in models that go beyond the mean-field level and include collective correlations. For instance, if rotational energy corrections and quadrupole fluctuations are treated explicitly by angular momentum projection and configuration mixing, they should not at the same time implicitly be included in the functional, i.e. through parameters adjusted to data that already include these correlations. Therefore, the parameters of such functionals must be adjusted to pseudodata, obtained by subtracting correlation effects from experimental masses and radii.

In the development of EDF-based structure models that include collective correlations through symmetry restorations and configuration mixing, relativistic functionals face the same challenges as their non-relativistic counterpart, i.e. Skyrme-type functionals. For these models to be able to make spectroscopic predictions in medium-heavy and heavy nuclei, often characterized by soft potential energy surfaces, it is important to build accurate and efficient algorithms that perform a complete restoration of symmetries broken by the static mean field (translational, rotational, particle number), and take into account fluctuations around the mean-field minima for very general shapes.

An interesting recent development, which goes beyond the scope of the present review, is the extension of the relativistic (Q)RPA to the quasiparticle time-blocking approximation [117–121]. This approach takes into account effects of particle-vibrational coupling and, therefore, enables a quantitative analysis of single-particle excitations in odd-mass nuclei and vibrational excitations. In particular, the dynamics of particle-vibrational coupling leads to an increase of the level density near the Fermi surface, i.e. to an enhancement of the nucleon effective mass. The RQRPA extended by the coupling to collective vibrations generates spectra with a multitude of two-quasiparticle-plus-phonon states, that are important in the description of damping phenomena characteristic for giant multipole excitations, as well as in studies of low-energy modes in neutron-rich nuclei.

Finally, interesting results could also be obtained by expanding nuclear energy density functionals to include non-nucleonic degrees of freedom. For instance, it has been shown that relativistic density functionals provide a natural framework for the description of hypernuclear single-particle spectra based on chiral SU(3) dynamics [122,123].

Acknowledgements

We would like to thank G.A. Lalazissis, Z.P. Li, Z.Y. Ma, J. Meng, L. Próchniak, Y. Tian, and J.M. Yao for their contribution to the work reviewed in this article. This work was supported in part by the MZOS—project 1191005-1010, and the DFG cluster of excellence "Origin and Structure of the Universe" (www.universe-cluster.de). T. N. acknowledges support by the Croatian Science Foundation.

References

[1] G.A. Lalazissis, P. Ring, D. Vretenar (Eds.), Extended Density Functionals in Nuclear Structure Physics, in: Lecture Notes in Physics, vol. 641, Springer, Heidelberg, 2004.
[2] M. Bender, P.-H. Heenen, P.-G. Reinhard, Rev. Modern Phys. 75 (2003) 121.
[3] W. Kohn, L.J. Sham, Phys. Rev. 140 (1965) A1133.
[4] W. Kohn, Rev. Modern Phys. 71 (1999) 1253.
[5] R.M. Dreizler, E.K.U. Gross, Density Functional Theory, Springer, Berlin, 1990.
[6] J.E. Drut, R.J. Furnstahl, L. Platter, Prog. Part. Nucl. Phys. 64 (2010) 120.
[7] D. Vretenar, Eur. Phys. J. Spec. Top. 156 (2008) 37.
[8] B.D. Serot, J.D. Walecka, Adv. Nucl. Phys. 16 (1986) 1.
[9] B.D. Serot, J.D. Walecka, Internat. J. Modern Phys. E 6 (1997) 515.
[10] R.J. Furnstahl, B.D. Serot, Comments Nucl. Part. Phys. 2 (2000) A23.
[11] J.N. Ginocchio, Phys. Rep. 414 (2005) 165.
[12] D. Vretenar, A.V. Afanasjev, G.A. Lalazissis, P. Ring, Phys. Rep. 409 (2005) 101.
[13] J. Meng, H. Toki, S.G. Zhou, S.Q. Zhang, W.H. Long, L.S. Geng, Prog. Part. Nucl. Phys. 57 (2006) 470.
[14] N. Paar, D. Vretenar, E. Khan, G. Colò, Rep. Progr. Phys. 70 (2007) 691.
[15] T. Nikšić, D. Vretenar, P. Ring, Phys. Rev. C 73 (2006) 034308.
[16] T. Nikšić, D. Vretenar, P. Ring, Phys. Rev. C 74 (2006) 064309.
[17] T. Nikšić, Z.P. Li, D. Vretenar, L. Próchniak, J. Meng, P. Ring, Phys. Rev. C 79 (2009) 034303.
[18] J.M. Yao, J. Meng, P. Ring, D.P. Arteaga, Phys. Rev. C 79 (2009) 044312.
[19] J.M. Yao, J. Meng, P. Ring, D. Vretenar, Phys. Rev. C 81 (2010) 044311.
[20] G.A. Lalazissis, J. König, P. Ring, Phys. Rev. C 55 (1997) 540.

[21] W. Long, J. Meng, N.V. Giai, S.-G. Zhou, Phys. Rev. C 69 (2004) 034319.
[22] B.G. Todd-Rutel, J. Piekarewicz, Phys. Rev. Lett. 95 (2005) 122501.
[23] C. Fuchs, H. Lenske, H.H. Wolter, Phys. Rev. C 52 (1995) 3043.
[24] F. de Jong, H. Lenske, Phys. Rev. C 57 (1998) 3099.
[25] F. Hofmann, C.M. Keil, H. Lenske, Phys. Rev. C 64 (2001) 034314.
[26] S. Typel, H.H. Wolter, Nuclear Phys. A 656 (1999) 331.
[27] T. Nikšić, D. Vretenar, P. Finelli, P. Ring, Phys. Rev. C 66 (2002) 024306.
[28] G.A. Lalazissis, T. Nikšić, D. Vretenar, P. Ring, Phys. Rev. C 71 (2005) 024312.
[29] D.G. Madland, B.A. Nikolaus, T. Hoch, Phys. Rev. C 46 (1992) 1757.
[30] T. Hoch, D. Madland, P. Manakos, T. Mannel, B.A. Nikolaus, D. Strottman, Phys. Rep. 242 (1994) 253.
[31] J.L. Friar, D.G. Madland, B.W. Lynn, Phys. Rev. C 53 (1996) 3085.
[32] J.J. Rusnak, R.J. Furnstahl, Nuclear Phys. A 627 (1997) 495.
[33] T. Bürvenich, D.G. Madland, J.A. Maruhn, P.-G. Reinhard, Phys. Rev. C 65 (2002) 044308.
[34] T. Nikšić, D. Vretenar, P. Ring, Phys. Rev. C 78 (2008) 034318.
[35] T. Nikšić, G.A. Lalazissis, D. Vretenar, P. Ring, Phys. Rev. C 77 (2008) 034302.
[36] P. Hohenberg, W. Kohn, Phys. Rev. 136 (1964) B864.
[37] P. Finelli, N. Kaiser, D. Vretenar, W. Weise, Nuclear Phys. A 735 (2004) 449.
[38] P. Finelli, N. Kaiser, D. Vretenar, W. Weise, Nuclear Phys. A 770 (2006) 1.
[39] S. Fritsch, N. Kaiser, W. Weise, Nuclear Phys. A 750 (2005) 259.
[40] W. Long, J. Meng, N. Van Giai, S.-G. Zhou, Phys. Rev. C 69 (2004) 034319.
[41] W. Long, N. Van Giai, J. Meng, Phys. Lett. B 640 (2006) 150.
[42] O. Plohl, C. Fuchs, Phys. Rev. C 74 (2006) 034325.
[43] O. Plohl, C. Fuchs, E.N.E. van Dalen, Phys. Rev. C 73 (2006) 014003.
[44] D.R. Entem, R. Machleidt, Phys. Rev. C 68 (2003) 041001(R).
[45] A. Akmal, V.R. Pandharipande, D.G. Ravenhall, Phys. Rev. C 58 (1998) 1804.
[46] R.J. Furnstahl, Nuclear Phys. A 706 (2002) 85.
[47] D. Vretenar, T. Nikšić, P. Ring, Phys. Rev. C 68 (2003) 024310.
[48] M. Baranger, K. Kumar, Nuclear Phys. A 110 (1968) 490.
[49] M. Kortelainen, T. Lesinski, J. Moré, W. Nazarewicz, J. Sarich, N. Schunck, M.V. Stoitsov, S. Wild, Phys. Rev. C 82 (2010) 024313.
[50] S. Goriely, M. Samyn, J.M. Pearson, Phys. Rev. Lett. 102 (2009) 152503.
[51] P. Klüpfel, P.-G. Reinhard, T.J. Bürvenich, J.A. Maruhn, Phys. Rev. C 79 (2009) 034310.
[52] M. Bender, G.F. Bertsch, P.-H. Heenen, Phys. Rev. C 73 (2006) 034322.
[53] M. Bender, G.F. Bertsch, P.-H. Heenen, Phys. Rev. C 69 (2004) 034340.
[54] P. Ring, Prog. Part. Nucl. Phys. 37 (1996) 193.
[55] M. Serra, P. Ring, Phys. Rev. C 65 (2002) 064324.
[56] J.F. Berger, M. Girod, D. Gogny, Nuclear Phys. A 428 (1984) 23c.
[57] J.F. Berger, M. Girod, D. Gogny, Comput. Phys. Comm. 63 (1991) 365.
[58] Y. Tian, Z.Y. Ma, P. Ring, Phys. Lett. B 676 (2009) 44.
[59] Y. Tian, Z.Y. Ma, P. Ring, Phys. Rev. C 79 (2009) 064301.
[60] Y. Tian, Z.Y. Ma, P. Ring, Phys. Rev. C 80 (2009) 024313.
[61] T. Nikšić, P. Ring, D. Vretenar, Y. Tian, Z.Y. Ma, Phys. Rev. C 81 (2010) 054318.
[62] P. Ring, P. Schuck, The Nuclear Many-Body Problem, Springer-Verlag, Heidelberg, 1980.
[63] A. Staszcak, M. Stoitsov, A. Baran, W. Nazarewicz, Eur. Phys. J. A 46 (2010) 85.
[64] G. Audi, A.H. Wapstra, C. Thibault, Nuclear Phys. A 729 (2003) 337.
[65] S. Raman, C.W. Nestor Jr., P. Tikkanen, At. Data Nucl. Data Tables 78 (2001) 1.
[66] A. Baran, Z. Lojewski, K. Sieja, M. Kowal, Phys. Rev. C 72 (2005) 044310.
[67] Z.P. Li, T. Nikšić, D. Vretenar, P. Ring, J. Meng, Phys. Rev. C 81 (2010) 064321.
[68] S. Bjørnholm, J.E. Lynn, Rev. Modern Phys. 52 (1980) 725.
[69] R.B. Firestone, V.S. Shirley, S.Y.F. Chu, C.M. Baglin, J. Zipkin, Table of Isotopes, John Wiley & Sons, New York, 1996.
[70] K.E.G. Löbner, M. Vetter, V. Hönig, Nucl. Data Tables A 7 (1970) 495.
[71] C.E. Bemis Jr., F.K. McGowan, J.L.C. Ford Jr., W.T. Milner, P.H. Stelson, R.L. Robinson, Phys. Rev. C 8 (1973) 1466.
[72] J.-P. Delaroche, M. Girod, H. Goutte, J. Libert, Nuclear Phys. A 771 (2006) 103.
[73] R. Rodríguez-Guzmán, J.L. Egido, L.M. Robledo, Phys. Rev. C 65 (2002) 024304.
[74] R. Rodríguez-Guzmán, J.L. Egido, L.M. Robledo, Nuclear Phys. A 709 (2002) 201.
[75] R. Rodríguez-Guzmán, J.L. Egido, L.M. Robledo, Phys. Rev. C 69 (2004) 054319.
[76] T.R. Rodríguez, J.L. Egido, Phys. Rev. Lett. 99 (2007) 062501.
[77] T.R. Rodríguez, J.L. Egido, Phys. Lett. B 663 (2008) 49.
[78] T.R. Rodríguez, J.L. Egido, Phys. Rev. C 81 (2010) 064323.
[79] A. Valor, P.-H. Heenen, P. Bonche, Nuclear Phys. A 671 (2000) 145.
[80] M. Bender, H. Flocard, P.-H. Heenen, Phys. Rev. C 68 (2003) 044321.
[81] T. Duguet, M. Bender, P. Bonche, P.-H. Heenen, Phys. Lett. B 559 (2003) 201.
[82] M. Bender, P. Bonche, T. Duguet, P.-H. Heenen, Phys. Rev. C 69 (2004) 064303.
[83] M. Bender, P. Bonche, P.-H. Heenen, Phys. Rev. C 74 (2006) 024312.
[84] M. Bender, P.-H. Heenen, Phys. Rev. C 78 (2008) 024309.
[85] T. Nikšić, D. Vretenar, G.A. Lalazissis, P. Ring, Phys. Rev. Lett. 99 (2007) 092502.
[86] M. Anguiano, J.L. Egido, L.M. Robledo, Nuclear Phys. A 696 (2001) 467.
[87] J. Dobaczewski, M. Stoitsov, W. Nazarewicz, P.-G. Reinhard, Phys. Rev. C 76 (2007) 054315.
[88] D. Lacroix, T. Duguet, M. Bender, Phys. Rev. C 79 (2009) 044318.
[89] M. Bender, T. Duguet, D. Lacroix, Phys. Rev. C 79 (2009) 044319.
[90] M. Baranger, M. Veneroni, Ann. Phys. NY 114 (1978) 123.
[91] P.-G. Reinhard, K. Goeke, Rep. Progr. Phys. 50 (1987) 1.
[92] P. Bonche, J. Dobaczewski, H. Flocard, P.-H. Heenen, J. Meyer, Nuclear Phys. A 510 (1990) 466.
[93] L. Próchniak, S.G. Rohoziński, J. Phys. G 36 (2009) 123101.
[94] B. Giraud, B. Grammaticos, Nuclear Phys. A 255 (1975) 141.
[95] M. Girod, B. Grammaticos, Nuclear Phys. A 330 (1979) 40.
[96] K. Goeke, P.-G. Reinhard, Ann. Phys. NY 124 (1980) 249.
[97] R.E. Peierls, J. Yoccoz, Proc. Phys. Soc. A 70 (1957) 381.
[98] D.J. Thouless, J.G. Valatin, Nuclear Phys. 31 (1962) 211.
[99] D.R. Inglis, Phys. Rev. 103 (1956) 1786.
[100] J. Libert, M. Girod, J.-P. Delaroche, Phys. Rev. C 60 (1999) 054301.
[101] E. Clément, et al., Phys. Rev. C 75 (2007) 054313.

[102] L. Próchniak, P. Quentin, D. Samsoen, J. Libert, Nuclear Phys. A 730 (2004) 59.
[103] J.-P. Delaroche, M. Girod, J. Libert, H. Goutte, S. Hilaire, S. Péru, N. Pillet, G.F. Bertsch, Phys. Rev. C 81 (2010) 014303.
[104] L. Próchniak, P. Ring, Internat. J. Modern Phys. E 13 (2004) 217.
[105] Z.P. Li, T. Nikšić, D. Vretenar, J. Meng, G.A. Lalazissis, P. Ring, Phys. Rev. C 79 (2009) 054301.
[106] Z.P. Li, T. Nikšić, D. Vretenar, J. Meng, Phys. Rev. C 80 (2009) 061301.
[107] Z.P. Li, T. Nikšić, D. Vretenar, J. Meng, Phys. Rev. C 81 (2010) 034316.
[108] K. Kumar, M. Baranger, Nuclear Phys. A 92 (1967) 608.
[109] L.M. Robledo, R. Rodríguez-Guzmán, P. Sarriguren, J. Phys. G 36 (2009) 115104.
[110] R. Rodríguez-Guzmán, P. Sarriguren, L.M. Robledo, J.E. García-Ramos, Phys. Rev. C 81 (2010) 024310.
[111] C. Ekström, et al., Nuclear Phys. A 348 (1980) 25.
[112] S. Ćwiok, P.-H. Heenen, W. Nazarewicz, Nature 433 (2005) 705.
[113] F. Iachello, Phys. Rev. Lett. 87 (2001) 052502.
[114] F. Iachello, Phys. Rev. Lett. 85 (2000) 3580.
[115] J.P. Perdew, A. Ruzsinszky, J. Tao, V.N. Staroverov, G.E. Scuseria, G.I. Csonka, J. Chem. Phys. 123 (2005) 062201.
[116] E. Epelbaum, H.-W. Hammer, Ulf-G. Meißner, Rev. Modern Phys. 81 (2009) 1773.
[117] E. Litvinova, P. Ring, Phys. Rev. C 73 (2006) 044328.
[118] E. Litvinova, P. Ring, V.I. Tselyaev, Phys. Rev. C 75 (2007) 064308.
[119] E. Litvinova, P. Ring, D. Vretenar, Phys. Lett. B 647 (2007) 111.
[120] E. Litvinova, P. Ring, V.I. Tselyaev, Phys. Rev. C 78 (2008) 014312.
[121] E. Litvinova, P. Ring, V.I. Tselyaev, K. Langanke, Phys. Rev. C 79 (2009) 054312.
[122] P. Finelli, N. Kaiser, D. Vretenar, W. Weise, Phys. Lett. B 658 (2007) 90.
[123] P. Finelli, N. Kaiser, D. Vretenar, W. Weise, Nuclear Phys. A 831 (2009) 163.